Ship Hidrodynamics

E. Oñate
J. García
S.R. Idelsohn

Chapter of the book *Encyclopedia of Computational Mechanics*.
E. Stein, R. de Borst and T.J.R. Hughes (Eds.)

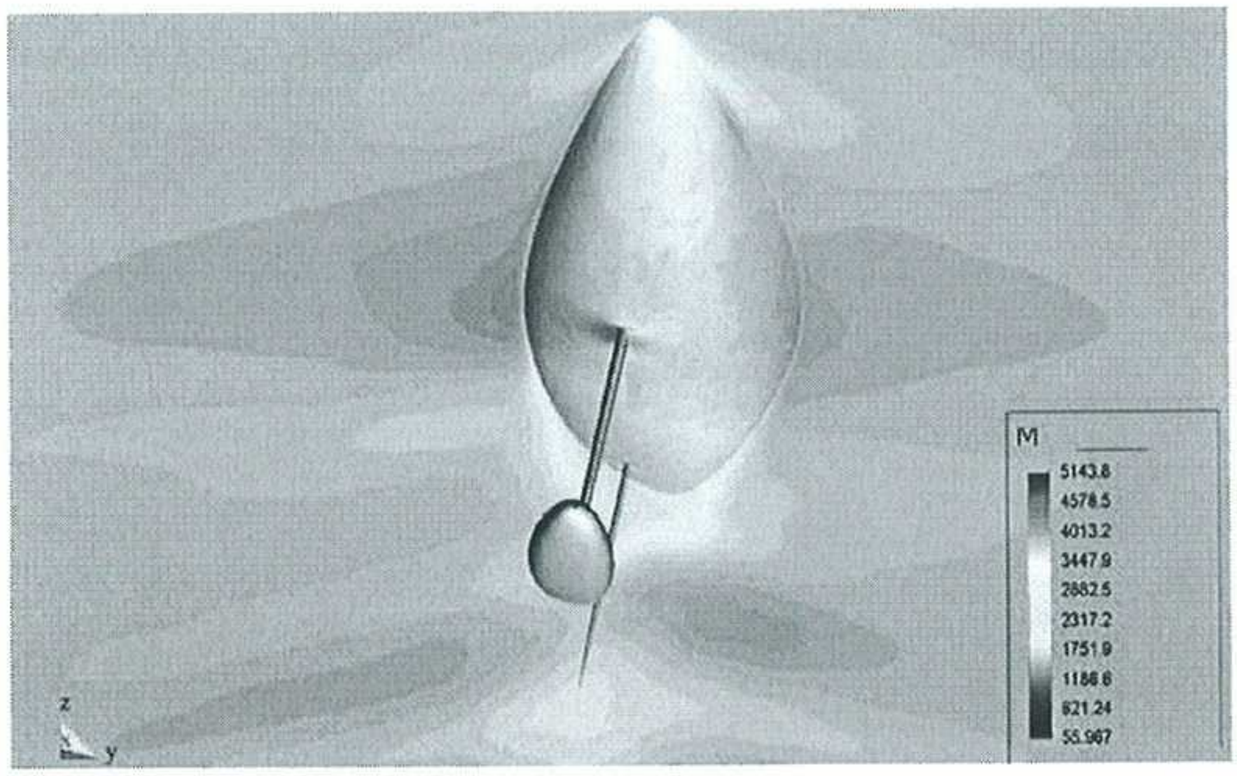

Publication CIMNE Nº-222, March 2003

Ship Hidrodynamics

E. Oñate
J. García
S.R. Idelsohn

Publication CIMNE Nº-222, March 2003

To be published in the *Encyclopedia of Computational Mechanics.*
Edited by Erwin Stein, René de Borst and Thomas J.R. Hughes

International Center for Numerical Methods in Engineering
Gran Capitán s/n, 08034 Barcelona, Spain

Ship hydrodynamics

Eugenio Oñate[1], Julio García[1] and Sergio R. Idelsohn[2]

[1] *International Center for Numerical Methods in Engineering (CIMNE) Universitat Politécnica de Catalunya (UPC), Gran Capitán, s/n, 08034 Barcelona, Spain*
[2] *CIMNE and International Center for Computational Methods in Engineering (CIMEC) Universidad Nacional del Litoral and CONICET, Santa Fe, Argentina*

ABSTRACT

This chapter presents an overview of some computational methods for analysis of ship hydrodynamics problems. Attention is focused on the description of a stabilized finite element formulation derived via a finite calculus procedure. Both arbitrary lagrangian-eulerian (ALE) and fully lagrangian forms are presented. Detailes of the treatment of the free surface waves and the interaction between the ship structure and the sea are also given. Examples of application to a variety of ship hydrodynamics problems are shown.

KEY WORDS: Ship hydrodynamics, finite element method, finite calculus, fluid-structure interaction

1. INTRODUCTION

Accurate prediction of the sea forces on a ship in motion is of paramount importance in ship design. The water resistance at a certain speed determines the required engine power and thereby the fuel consumption. Minimization of the hydrodynamic forces is therefore an important issue in ship hull design. Further, excitation of a wave pattern by ship motion not only induces wave resistance but may also limit the speed in the vecinity of the shore for environmental reasons, which must also be taken into account in ship design.

The usual simplification in ship hydrodynamics design is to separately consider the performance of the ship in still water and its behaviour in open sea. Hydrodynamic optimisation of a hull primarily requires the calculation of the resistance in a calm sea and the open sea effects are generally taken into account as a wave added resistance.

The resistance of a ship in still water can be considered as the sum of several contributions: a viscous resistance associated with the generation of boundary layers, the wave resistance, the air resistance on the superstructure and the induced resistance related to the generation of lift forces.

Wave resistance in practical cases amounts to 10 to 60 % of the total resistance of a ship in still water (Raven, 1996). It increases very rapidly at high speeds dominating the viscous component for fast displacement ships. Furthermore, wave resistance is very sensitive to the hull form design and easily affected by small shape modifications. For all these reasons, the possibility to predict and reduce the wave resistance is an important target.

Encyclopedia of Computational Mechanics. Edited by Erwin Stein, René de Borst and Thomas J.R. Hughes.

The prediction of the wave pattern and the wave resistance of a ship has challenged mathematicians and hydrodynamicists for over a century. The Boundary Element Method (BEM) is the basis of many computational algorithms developed in past years. Here the flow problem is solved using a simple potential model. BEM methods, termed by hydrodynamicists as Panel Methods may be classified into two categories. The first one uses the Kelvin wave source as the elementary singularity. The main advantage of such scheme is the automatic satisfaction of the radiation condition. The theoretical background of this method was reviewed by Wehausen (1970), while computational aspects can be found in Soding (1996) and Jenson and Soding (1989). The second class of BEM schemes uses the Rankine source as the elementary singularity. This procedure, first presented by Dawson (1977), has been widely applied in practice and many improvements have been addressed to account for the nonlinear wave effects. Among these, a succesful example is the Rankine Panel Method (Xia, 1986; Jenson and Soding, 1989; Nakos and Sclavounos, 1990).

In addition to the important developments in potential flow panel methods for practical ship hydrodynamics analysis during the period 1960–1980, much research in the second half of the twentieth century was oriented towards the introduction of viscosity in the CFD analysis. In the 1960's the viscous flow research was mainly focused in 2D boundary layer theory and by the end of the decade several methods for arbitrary pressure gradients were available. This research continued to solve the 3D case during the following decade and an evaluation of the capability of the new methods to predict ship wave resistance was carried out at different workshops (Bai and McCarthy, 1979; Larson, 1981; Noblesse and McCarthy, 1983). Here application to some well specified test cases were reported and numerical and experimental results compared acceptable well for most part of the boundary layer along the hull, while wrong results were obtained near the stern. This prompted additional research and by the end of the 1980's a number of numerical procedures for solving the full viscous flow equation accounting for simple turbulence modes based on Reynolds averaged Navier-Stokes (RANS) equations were available. Considerable improvements for predicting the stern flow were reported in subsequent workshops organized in the 1990's (Kim and Lucas, 1990; Reed *et al.*, 1990; Raven, 1992; Beck *et al.*, 1993; Soding, 1996; Janson and Larsson, 1996; Alessandrini and Delhommeau, 1996; Miyata, 1996). A good review of the status of CFD in ship hydrodynamics in the last part of the 20th century can be found in Larsson *et al.* (1998).

Independently of the flow equations used, the free surface boundary condition has been solved in different manners. The exact free surface condition is nonlinear and several linearizations have been proposed (Baba and Takekuma, 1975; Newmann, 1976; Idelsohn *et al.*, 1999). Some of them use a fixed domain and others a moving one. An alternative is to solve the full nonlinear free surface equation on a reference surface which does not necessary coincides with the free surface itself. In this way the updating of the surface mesh is minimized and sometimes is not even necessary.

The solution of the free surface equation in a bounded domain brings in the necessity of a radiation condition to eliminate spurious waves. A way to introduce this condition was proposed by Dawson (1977) who used a finite difference (FD) formula based in four upwind points to evaluate the first derivatives appearing in the free surface equation. This method became very popular and this is probably the main reason why a large majority of codes predicting the wave resistance of ships use FD methods on structured meshes (Larsson *et al.*, 1998).

Indeed the 1990's were a decade of considerable progress in CFD methods for ship

Encyclopedia of Computational Mechanics. Edited by Erwin Stein, René de Borst and Thomas J.R. Hughes.

hydrodynamics and the most important breakthrough was perhaps the coupled solution of the free surface equation with the fluid flow equations. Here a number of viscous and inviscid solutions for the surface ship wave problem using finite element (FE) and finite volume (FV) methods with non structured grids were reported (Farmer *et al.*, 1993, Hino *et al.*, 1993; García, 1995; Luo *et al.*, 1995; García, 1998; Storti *et al.*, 1998a, 1998b; Idelsohn *et al.*, 1999; Löhner, 1999).

The current challenges in CFD research for ship hydrodynamics focus in the development of robust (stable) and computationaly efficient numerical methods able to capture the different scales involved in the analysis of practical ship hydrodynamics situations. Wave resistance coefficients for modern ship design are needed for a wide range of speeds and here the accurate prediction of the wave pattern and the hull pressure distribution at low speed (say below Froude number $(Fn) = 0{,}2$) are still major challenges. Great difficulties also exist in the computation of the viscous resistance which requires very fine grids in the vecinity of the hull, resulting in overall meshes involving (at least) some $10^7 - 10^9$ elements. Other relevant problems are the prediction of the wake details and the propeller-hull interaction. Fine meshing and advanced turbulence models are crucial for the realistic solution of these problems. Indeed the use of unstructured meshes is essential for problems involving complex shapes.

A different class of ship hydrodynamic problems require taking beyond its limits the assumption of continuum mechanics. These situations are found in the modelling of breaking waves, or in the prediction of water inside the hull (green water) due to large amplitude waves typical of sea keeping problems. Here lagrangian flow methods where the motion of each flow particle is individually tracked using techniques developed for (incompressible) solid mechanics are a promising trend for solving a wide class of ship hydrodynamics problems.

The content of the chapter is structured as follows. In the next section the standard Navier-Stokes equations for an incompressible viscous flow are presented. The equations are formulated in an arbitrary lagrangian-eulerian (ALE) description allowing the independent motion of the mesh nodes from that of the fluid particles. Details of the problems posed by the free surface wave boundary condition are given. The difficulties encountered in the numerical solution of the fluid flow and the free surface equations, namely the unstabilities induced by the convective terms and the limits in the approximation introduced by the incompressibility constraint are explained. A new procedure for deriving stabilized numerical methods for this type of problems based on the so called *finite calculus* (FIC) formulation is presented. The FIC method is based in redefining the standard governing equations in fluid mechanics by expressing the balance laws in a domain of *finite size*. This introduces additional terms in the differential equations of the infinitessimal theory which are essential to derive stabilized numerical schemes (Oñate, 1996, 2002). We present here a stabilized finite element method using equal order linear interpolation for the velocity and the pressure variables. Both monolithic and fractional step time integration procedures are described. A method for solving the coupled fluid-structure interaction problem induced by the motion of the ship due to the sea forces is also presented. A mesh moving algorithm for updating the position of the free surface nodes during the ship motion is given.

In the last part of the chapter the lagrangian formulation for fluid flow analysis is presented as a particular case of the ALE form. The lagrangian description has particular advantages for tracking the displacement of the fluid particles in flows where large motions of the fluid surface occur. One of the advantages of the lagrangian approach is that the convective terms dissapear in the governing equations of the fluid. In return, the updating of the mesh at almost every

Encyclopedia of Computational Mechanics. Edited by Erwin Stein, René de Borst and Thomas J.R. Hughes.

time step is now a necessity and efficient mesh generation algorithms must be used (Idelsohn *et al.*, 2002a,b,c).

The examples show the efficiency of the eulerian, ALE and fully lagrangian formulations to solve a variety of ship hydrodynamics problems.

2. THE NAVIER-STOKES EQUATIONS FOR INCOMPRESSIBLE FLOWS. ALE FORMULATION

2.1. Momentum and mass conservation equations

The Navier-Stokes equations for an incompressible fluid in a domain Ω can be written in an arbitrary lagrangian-eulerian form as

Momentum

$$\boxed{\rho\left(\frac{\partial u_i}{\partial t}+v_j\frac{\partial u_i}{\partial x_j}+u_i\frac{\partial u_j}{\partial x_j}\right)+\frac{\partial p}{\partial x_i}-\frac{\partial s_{ij}}{\partial x_j}-b_i=0} \quad \text{in } \Omega \tag{1}$$

Mass conservation

$$\boxed{\frac{\partial u_i}{\partial x_i}=0} \quad \text{in } \Omega \tag{2}$$

In Eq.(1) u_i is the velocity along the ith global reference axis, u_i^m is the velocity of the moving mesh nodes, $v_i = u_i - u_i^m$ is the relative velocity between the fluid and the moving mesh nodes ρ is the (constant) density of the fluid, b_i are body forces, t is the time, p is the pressure and s_{ij} are the viscous stresses related to the viscosity μ by the standard expression

$$s_{ij}=2\mu\left(\varepsilon_{ij}-\frac{1}{3}\delta_{ij}\frac{\partial u_k}{\partial x_k}\right) \tag{3}$$

where δ_{ij} is the Kronecker delta and the strain rates ε_{ij} are

$$\varepsilon_{ij}=\frac{1}{2}\left(\frac{\partial u_i}{\partial x_j}+\frac{\partial u_j}{\partial x_i}\right) \tag{4}$$

The presence of the volumetric strain rate terms in the Eqs.(1) and (3) are useful for the derivation of the stabilized formulation in Section 5.

Eqs.(1)–(3) are completed with the boundary conditions

$$n_j\sigma_{ij}-t_i=0 \quad \text{on } \Gamma_t \tag{5a}$$

$$u_j-u_j^p=0 \quad \text{on } \Gamma_u \tag{5b}$$

where $\sigma_{ij}=s_{ij}-p\delta_{ij}$ are the total stresses, n_j are the component of the unit normal vector to the boundary and t_i and u_j^p are prescribed tractions and velocities on the Neumann and

Encyclopedia of Computational Mechanics. Edited by Erwin Stein, René de Borst and Thomas J.R. Hughes.

Dirichlet boundaries Γ_t and Γ_u, respectively where $\Gamma = \Gamma_t \cup \Gamma_u$ is the boundary of the analysis domain Ω. The boundary conditions are completed with the initial condition $u_j = u_j^0$ for $t = t_0$.

In above equations $i, j = 1, n_d$ where n_d is the number of space dimension (i.e. $n_d = 3$ for 3D). Also, throughout the text the summation convention for repeated indexes is assumed unless specified otherwise.

2.2. Free surface boundary conditions

The boundary conditions (5a) on the surface tractions can be written in local normal and tangential axes as

$$\begin{aligned} &\sigma_n - t_n = 0 \\ &\sigma_{t_j} - \bar{t}_{g_j} = 0 \qquad j = 1,2 \quad \text{for 3D} \end{aligned} \tag{6}$$

where σ_n and σ_{t_j} are the normal and tangential stresses, respectively and t_n and t_{g_j} are the prescribed normal and tangential tractions, respectively.

On the free boundary we have to ensure at all times that: 1) the pressure (which approximates the normal stres) equals the atmospheric pressure and the tangential tractions are zero unless specified otherwise, and 2) material particles of the fluid belong to the free surface.

The condition on the pressure is simply especified as

$$p = p_a \tag{7}$$

where p_a is the atmospheric pressure (usually given a zero value).

The condition on the tangential tractions is satisfied by setting $t_{g_i} = 0$ in Eq.(6). This is automatically accounted for by the *natural boundary conditions* in the weak form of the momentum equations (Zienkiewicz and Taylor Vol. 3, 2000).

The condition on the material particles is expressed (for steady state conditions) as

$$u_i n_i = 0 \qquad \text{or} \qquad \mathbf{u}^T \mathbf{n} = 0 \tag{8}$$

i.e. the velocity vector is tangent to the free surface. Eq.(8) can be rewritten noting that the normal vector has the following components

$$\mathbf{n} = \left[-\frac{\partial \beta}{\partial x_1}, 1 \right]^T \quad \text{for 2D} \quad \text{and} \quad \mathbf{n} = \left[-\frac{\partial \beta}{\partial x_1}, -\frac{\partial \beta}{\partial x_2}, 1 \right]^T \quad \text{for 3D} \tag{9}$$

In Eq.(9) $\beta = x_3 - x_3^{\text{ref}}$ is the free surface elevation measured in the direction of the vertical coordinate x_3 relative to some previously known surface, which we shall refer to as the *reference surface* (Figure 2). This surface may be horizontal (i.e. the undisturbed water surface) or may be simply a previously computed surface.

Introducing Eq.(9) into (8) gives (for 3D)

$$u_i \frac{\partial \beta}{\partial x_i} - u_3 = 0 \quad , \quad i = 1,2 \tag{10}$$

Encyclopedia of Computational Mechanics. Edited by Erwin Stein, René de Borst and Thomas J.R. Hughes.

Eq.(10) is generalized for the transient case as

$$\boxed{\frac{\partial \beta}{\partial t} + u_i \frac{\partial \beta}{\partial x_i} - u_3 = 0} \quad , \quad i = 1, 2 \tag{11}$$

We observe that β obeys *a pure convection* equation with u_3 playing the role of a (non linear) source term. The solution of Eq.(11) with standard Galerkin FEM, or centred FD or FV methods will therefore suffer from numerical instabilities and some kind of stabilization is needed in order to obtain a physically meaningful solution. A method to solve Eq.(11), very popular in the context of the potential flow formulation, was introduced by Dawson (1977) using a four point FD upwind operator to evaluate the first derivatives of β on regular grids. Dawson's method has been extended by different authors to solve a many ship hydrodynamics problems (Raven, 1996; Larsson *et al.*, 1998; Idelsohn *et al.*, 1999).

Solution of Eq.(11) is strongly coupled with that of the fluid flow equations. The solution of the whole problem is highly non linear due to the pressence of the unknown velocities in Eq.(11) and also to the fact that the free surface position defining the new boundary conditions is also unknown. A number of iterative schemes have been developed for the solution of the non linear surface wave problem (Idelsohn *et al.*, 1999). They all basically involve solving Eq.(11) for the new free surface height β, for fixed values of the velocity field computed from the fluid solver in a previous iteration within each time increment. At this stage two procedures are possible, either the position of the free surface is updated after each iteration and this becomes the new reference surface, or else an equivalent pressure of value $p = p_a + |g|(\beta - \beta_{\text{ref}})$, where g is the gravity constant, is applied at the current reference surface as a boundary condition in the next flow iteration. The first option might require the regeneration of a new mesh, whereas the second one is less accurate but computationaly cheaper. Hence a compromise between the two alternative is usually chosen in practice. The iterative process continues until a converged solution is found for the velocity, the pressure and the free surface height at each time step. Details of the computational process are described in a next section.

An alternative method to treat the free surface equation is based in the volume of fluid (VOF) technique (Hirt and Nichols, 1981). In the VOF method the free surface position is defined as the interface between two fluids interacting with each other, where the efect of one fluid on the other is very small (i.e. the water and the surrounding air). An interface function which takes the values 0 and 1 for each of the two fluids is transported with the fluid velocity using a time dependent advection equation. Examples of application of the VOF to ship hydrodynamics problems can be found in Aliabadi and Shujaee (2001) and Aliabadi *et al.* (2002).

3. ABOUT THE FINITE ELEMENT SOLUTION OF THE NAVIER-STOKES EQUATIONS

The development of efficient and robust numerical methods for incompressible flow problems has been a subject of intensive research in last decades. Much effort has been spent in developing the so called stabilized numerical methods overcoming the two main sources of

Encyclopedia of Computational Mechanics. Edited by Erwin Stein, René de Borst and Thomas J.R. Hughes.

instability in incompressible flow analysis, namely those originated by the high values of the convective terms and those induced by the difficulty in satisfying the incompressibility constraint.

The solution of above problems in the context of the finite element method (FEM) has been attempted in a number of ways. The underdiffusive character of the Galerkin FEM for high convection flows (which incidentaly also occurs for centred FD and FV methods) has been corrected by adding some kind of artificial viscosity terms to the standard Galerkin equations (Zienkiewicz and Taylor, Vol. 3 2000).

A popular way to overcome the problems with the incompressibility constraint is by introducing a pseudo-compressibility in the flow and using implicit and explicit algorithms developed for this kind of problems, such as artificial compressibility schemes (Chorin, 1967; Farmer *et al.*, 1993; Peraire *et al.*, 1994; Briley *et al.*, 1995; Sheng *et al.*, 1996) and preconditioning techniques (Idelsohn *et al.*, 1995). Other FEM schemes with good stabilization properties for the convective and incompressibility terms are based in Petrov-Galerkin (PG) techniques. The background of PG methods are the non-centred (upwind) schemes for computing the first derivatives of the convective operator in FD and FV methods. More recently a general class of Galerkin FEM has been developed where the standard Galerkin variational form is extended with adequate residual-based terms in order to achieve a stabilized numerical scheme (Codina, 1998, 2000). Among the many FEM of this kind we can name the Streamline Upwind Petrov Galerkin (SUPG) method (Brooks and Hughes, 1982; Hughes and Mallet, 1986; Idelsohn *et al.*, 1995; Storti *et al.*, 1995, 1997; Cruchaga and Oñate, 1997, 1999), the Galerkin Least Square (GLS) method (Hughes *et al.*, 1989; Tezduyar, 1991; Tezduyar *et al.*, 1992a), the Taylor-Galerkin method (Donea, 1994), the Characteristic Galerkin method (Douglas and Russell, 1982; Pironneau, 1982; Löhner *et al.*, 1984) and its variant the characteristic Based Split (CBS) method (Zienkiewicz and Codina, 1995; Codina *et al.*, 1998; Codina and Zienkiewicz, 2002), pressure gradient operator methods (Codina and Blasco, 1997, 2002) and the Subgrid Scale (SS) method (Hughes, 1995; Brezzi *et al.*, 1997; Codina, 2000, 2002).

In this work a stabilized FEM for incompressible flows is derived taking as the starting point the modified governing equations of the flow problem formulated via a finite calculus (FIC) approach. The FIC method is based in invoking the balance of fluxes in a domain of finite size. This introduces naturally additional terms in the classical differential equations of infinitessimal fluid mechanics which are a function of the balance domain dimensions. The new terms in the modified governing equations provide naturally the necessary stabilization to the standard Galerkin finite element method.

In the next section, the main concepts of the FIC approch are introduced via a simple 1D convection-diffusion model problem. Then the FIC formulation of the fluid flow equations and the free surface wave equations using the finite element method are presented.

4. BASIC CONCEPTS OF THE FINITE CALCULUS (FIC) METHOD

We will consider a convection-diffusion problem in a 1D domain Ω of length L. The equation of balance of fluxes in a subdomain of size d belonging to Ω (Figure 1) is written as

$$q_A - q_B = 0 \tag{12}$$

Encyclopedia of Computational Mechanics. Edited by Erwin Stein, René de Borst and Thomas J.R. Hughes.

where q_A and q_B are the incoming and outgoing fluxes at points A and B, respectively. The flux q includes both convective and diffusive terms; i.e. $q = u\phi - k\frac{d\phi}{dx}$, where ϕ is the transported variable, u is the velocity and k is the diffusitivity of the material.

We express now the fluxes q_A and q_B in terms of the flux at an arbitrary point C within the balance domain (Figure 1). Expanding q_A and q_B in Taylor series around point C up to second order terms gives

$$q_A = q_C - d_1 \frac{dq}{dx}|_C + \frac{d_1^2}{2}\frac{d^2q}{dx^2}|_C + O(d_1^3) \quad , \quad q_B = q_C + d_2 \frac{dq}{dx}|_C + \frac{d_2^2}{2}\frac{d^2q}{dx^2}|_C + O(d_2^3) \tag{13}$$

Substituting Eq.(13) into Eq.(12) gives after simplification

$$\frac{dq}{dx} - \underline{\frac{h}{2}\frac{d^2q}{dx^2}} = 0 \tag{14}$$

where $h = d_1 - d_2$ and all derivatives are computed at point C.

Standard calculus theory assumes that the domain d is of infinitessimal size and the resulting balance equation is simply $\frac{dq}{dx} = 0$. We will relax this assumption and allow the balance domain to have a *finite size*. The new balance equation (14) incorporates now the underlined term which introduces the *characteristic length* h. Obviously, accounting for higher order terms in Eq.(13) would lead to new terms in Eq.(14) involving higher powers of h.

Distance h in Eq.(14) can be interpreted as a free parameter depending on the location of point C (note that $h = 0$ for $d_1 = d_2$). However, the fact that Eq.(14) is the exact balance equation (up to second order terms) for any 1D domain of finite size and that the position of point C is arbitrary, can be used to derive numerical schemes with enhanced properties, simply by computing the characteristic length parameter using an adequate "optimality" rule.

Consider, for instance, the modified equation (14) applied to the convection-diffusion problem. Neglecting third order derivatives of ϕ, Eq.(14) can be written as

$$-u\frac{d\phi}{dx} + \left(k + \frac{uh}{2}\right)\frac{d^2\phi}{dx^2} = 0 \tag{15}$$

We see that the FIC procedure introduces *naturally* an additional diffusion term into the standard convection-diffusion equation. This is the basis of the popular "artificial diffusion" method (Hirsch, 1990). The characteristic length h is typically expressed as a function of the cell or element dimensions. The optimal or critical value of h can be computed from numerical stability conditions such as obtaining a physically meaningful solution, or even obtaining "exact" nodal values (Zienkiewicz and Taylor, 2000; Oñate and Manzan, 2000; Oñate, 2002).

Equation (13) can be extended to account for source and time effects. The full FIC equation for the transient convection-diffusion problem can be written in compact form as

$$r - \underline{\frac{h}{2}\frac{dr}{dx}} - \underline{\frac{\delta}{2}\frac{\partial r}{\partial t}} = 0 \tag{16}$$

$$r = -\left(\frac{d\phi}{dt} + u\frac{d\phi}{dx}\right) + \frac{d}{dx}\left(k\frac{d\phi}{dx}\right) + Q \tag{17}$$

where Q is the external source and δ is a time stabilization parameter (Oñate, 1998; Oñate and Manzan, 1999). For consistency a FIC form of the Neumann boundary condition should

Encyclopedia of Computational Mechanics. Edited by Erwin Stein, René de Borst and Thomas J.R. Hughes.

be used. This is obtained by invoking balance of fluxes in a domain of finite size next to the boundary Γ_q where the flux is prescribed to a value $\bar{q}$. The modified FIC boundary condition is

$$k\frac{d\phi}{dx} + \bar{q} - \underline{\frac{h}{2}r} = 0 \quad \text{at } \Gamma_q \tag{18}$$

The definition of the problem is completed with the standard Dirichlet condition prescribing the value of ϕ at the boundary Γ_ϕ and the initial conditions.

5. FIC EQUATIONS FOR VISCOUS INCOMPRESSIBLE FLOW. ALE FORMULATION

The starting point are the FIC equations for a viscous incompressible fluid. For simplicity we will neglect the time stabilization term, as this is not relevant for the purposes of this work. The equations are written as (Oñate, 1998, 2000; Oñate *et al.*, 2002)

Momentum

$$r_{m_i} - \underline{\frac{1}{2}h_j\frac{\partial r_{m_i}}{\partial x_j}} = 0 \tag{19}$$

Mass balance

$$\left(\frac{\partial u_k}{\partial x_k}\right) - \underline{\frac{h_j}{2}\frac{\partial}{\partial x_j}\left(\frac{\partial u_k}{\partial x_k}\right)} = 0 \tag{20}$$

where

$$r_{m_i} = \rho\left(\frac{\partial u_i}{\partial t} + v_j\frac{\partial u_i}{\partial x_j} + u_i\frac{\partial u_j}{\partial x_j}\right) + \frac{\partial p}{\partial x_i} - \frac{\partial s_{ij}}{\partial x_j} - b_i \qquad i,j = 1,n_d \tag{21}$$

and all the terms have been defined in Section 2.1.

The Neumann boundary conditions for the FIC formulation are (Oñate, 1998, 2000)

$$n_j\sigma_{ij} - t_i + \underline{\frac{1}{2}h_j n_j r_{m_i}} = 0 \quad \text{on } \Gamma_t \tag{22}$$

The Dirichlet and initial boundary conditions are the standard ones given in Section 2.1.

The $h_i's$ in above equations are characteristic lengths of the domain where balance of momentum and mass is enforced. In Eq.(22) these lengths define the domain where equilibrium of boundary tractions is established. The sign in front the h_i term in Eq.(22) is consistent with the definition of r_{m_i} in Eq.(21).

Eqs.(19)–(22) are the starting point for deriving stabilized FEM for solving the incompressible Navier-Stokes equations using equal order interpolation for all variables.

5.1. Stabilized integral forms

From Eqs.(19) and (3) it can be obtained

$$\frac{h_j}{2}\frac{\partial}{\partial x_j}\left(\frac{\partial u_k}{\partial x_k}\right) \simeq \sum_{i=1}^{n_d}\tau_i\frac{\partial r_{m_i}}{\partial x_i} \tag{23}$$

Encyclopedia of Computational Mechanics. Edited by Erwin Stein, René de Borst and Thomas J.R. Hughes.

where

$$\tau_i = \left(\frac{8\mu}{3h_i^2} + \frac{2\rho u_i}{h_i} \right)^{-1} \tag{24}$$

Substituting Eq.(23) into Eq.(20) leads to the following stabilized mass balance equation

$$\frac{\partial u_k}{\partial x_k} - \sum_{i=1}^{n_d} \tau_i \frac{\partial r_{m_i}}{\partial x_i} = 0 \tag{25}$$

The τ_i's in Eq.(23) are *intrinsic time parameters* which also appear in other stabilized formulations (Hughes and Mallet, 1986a; Tezduyar, 1991, 2001; Codina, 2002). Note that these parameters emerge naturally form the FIC formation and take the values of $\tau_i = \dfrac{3h_i^2}{8\mu}$ and $\tau_i = \dfrac{h_i}{2\rho u_i}$ for the viscous limit (Stokes flow) and the inviscid limit (Euler flow), respectively.

The weighted residual form of the governing equations (Eqs.(19), (22) and (25)) is

$$\int_\Omega \delta u_i \left[r_{m_i} - \frac{h_j}{2} \frac{\partial r_{m_i}}{\partial x_j} \right] + \int_{\Gamma_t} \delta u_i (\sigma_{ij} n_j - t_i + \frac{h_j}{2} n_j r_{m_i}) d\Gamma = 0 \tag{26}$$

$$\int_\Omega q \left[\frac{\partial u_k}{\partial x_k} - \sum_{i=1}^{n_d} \tau_i \frac{\partial r_{m_i}}{\partial x_i} \right] d\Omega = 0 \tag{27}$$

where δu_i and q are arbitrary weighting functions representing virtual velocity and virtual pressure fields, respectively. Integrating by parts above equations leads to

$$\int_\Omega \left[\delta u_i \rho \left(\frac{\partial u_i}{\partial t} + u_j \frac{\partial u_i}{\partial x_j} \right) + \delta \varepsilon_{ij} (\tau_{ij} - \delta_{ij} p) \right] d\Omega - \int_\Omega \delta u_i b_i d\Omega - \int_{\Gamma_t} \delta u_i t_i d\Omega + \sum_e \int_{\Omega^e} \frac{h_j}{2} \frac{\partial \delta u_i}{\partial x_j} r_{m_i} d\Omega = 0 \tag{28}$$

$$\int_\Omega q r_d \, d\Omega + \int_\Omega \left[\sum_{i=1}^{n_d} \tau_i \frac{\partial q}{\partial x_i} r_{m_i} \right] d\Omega = 0 \tag{29}$$

The fourth integral in Eq.(28) is computed as a sum of the element contributions to allow for discontinuities in the derivatives of r_{m_i} along the element interfaces. As usual $\delta \varepsilon_{ij} = \frac{1}{2} \left(\frac{\partial \delta u_i}{\partial x_j} + \frac{\partial \delta u_j}{\partial x_i} \right)$. Also in Eq.(28) we have neglected the volumetric strain rate tersm, whereas in the derivation of Eq.(29) we have assumed that r_{m_i} is negligible on the boundaries.

5.2. Convective and pressure gradient projections

The convective and pressure gradient projections c_i and π_i are defined as

$$c_i = r_{m_i} - \rho u_j \frac{\partial u_i}{\partial x_j} \tag{30}$$

$$\pi_i = r_{m_i} - \frac{\partial p}{\partial x_i} \tag{31}$$

Encyclopedia of Computational Mechanics. Edited by Erwin Stein, René de Borst and Thomas J.R. Hughes.

We can now express r_{m_i} in Eqs.(28) and (29) in terms of c_i and π_i, respectively which become additional variables. The system of integral equations is now augmented in the necessary number of equations by imposing that the residuals r_{m_i} vanish (in average sense) for both forms given by Eqs.(30) and (31). The final system of integral equations is:

$$\begin{aligned}
&\int_\Omega \left[\delta u_i \rho \left(\frac{\partial u_i}{\partial t} + u_j \frac{\partial u_i}{\partial x_j}\right) + \delta\varepsilon_{ij}(\tau_{ij} - \delta_{ij}p)\right] d\Omega - \int_\Omega \delta u_i b_i d\Omega - \int_{\Gamma_t} \delta u_i t_i d\Omega + \\
&\qquad + \sum_e \int_{\Omega^e} \frac{h_k}{2} \frac{\partial(\delta u_i)}{\partial x_k} \left(\rho u_j \frac{\partial u_i}{\partial x_j} + c_i\right) d\Omega = 0 \\
&\int_\Omega q \left(\frac{\partial u_k}{\partial x_k}\right) d\Omega + \int_\Omega \sum_{i=1}^{n_d} \tau_i \frac{\partial q}{\partial x_i} \left(\frac{\partial p}{\partial x_i} + \pi_i\right) d\Omega = 0 \\
&\int_\Omega \delta c_i \rho \left(\rho u_j \frac{\partial u_i}{\partial x_j} + c_i\right) d\Omega = 0 \qquad \text{no sum in } i \\
&\int_\Omega \delta\pi_i \tau_i \left(\frac{\partial p}{\partial x_i} + \pi_i\right) d\Omega = 0 \qquad \text{no sum in } i
\end{aligned} \tag{32}$$

where δc_i and $\delta\pi_i$ are appropriate weighting functions and the ρ and τ_i terms are introduced in the last two equations for convenience. As usual $i, j, k = 1, n_d$.

5.3. Stabilized FIC equations for the free surface wave condition

We will derive next the FIC equation for the water wave surface.

Let us consider a 2D free surface wave problem. Figure 3 shows a typical free surface segment line AB. The average vertical velocity for the segment $\bar{u}_2$ is defined as

$$\bar{u}_2 = \frac{u_2^A + u_2^B}{2} \tag{33a}$$

where u_2^A and u_2^B are the vertical velocities of the end points of the segment A and B.

The average vertical velocity $\bar{u}_2$ can be computed from the wave heights at points A and B as

$$\bar{u}_2 = \frac{x_2^B - x_2^A}{\bar{\delta}} \tag{33b}$$

where $\bar{\delta}$ is the time which a material particle takes to travel from point A to point B at the average velocity $\bar{u}_2$ and $x_2 \equiv \beta$ is the free surface wave height. Equaling Eq.(33a) and (33b) gives

$$\frac{u_2^A + u_2^B}{2} = \frac{x_2^B - x_2^A}{\bar{\delta}} \tag{33c}$$

We can now express the vertical velocities and the wave height at points A and B in terms

Encyclopedia of Computational Mechanics. Edited by Erwin Stein, René de Borst and Thomas J.R. Hughes.

of values at an arbitrary point C as

$$\begin{aligned}
u_2^A &= u_2(x_1^C - d_1, t^C - \delta_1) = u_2^C - d_1\frac{\partial\beta}{\partial x_1} - \delta_1\frac{\partial\beta}{\partial\delta_1} + O(d_1^2, t_1^2) \\
u_2^B &= u_2(x_1^C + d_2, t^C + \delta_2) = u_2^C + d_2\frac{\partial\beta}{\partial x_2} + \delta_2\frac{\partial\beta}{\partial\delta_2} + O(d_2^2, t_2^2) \\
x_2^A &= x_2(x_1^C - d_1, t^C - \delta_1) = x_2^C - d_1\frac{\partial\beta}{\partial x_1} - \delta_1\frac{\partial\beta}{\partial t} + \frac{d_1^2}{2}\frac{\partial^2\beta}{\partial x_1^2} + \\
&\quad + d_1\delta_1\frac{\partial^2\beta}{\partial x_1\partial t} + \frac{\delta_1^2}{2}\frac{\partial^2\beta}{\partial t^2} + O(d_1^3, \delta_1^3) \\
x_2^B &= x_2(x_1^C + d_2, t^C + \delta_2) = x_2^C + d_2\frac{\partial\beta}{\partial x_1} + \delta_2\frac{\partial\beta}{\partial t} + \frac{d_2^2}{2}\frac{\partial^2\beta}{\partial x_1^2} + \\
&\quad + d_2\delta_2\frac{\partial^2\beta}{\partial x_1\partial t} + \frac{\delta_2^2}{2}\frac{\partial^2\beta}{\partial t^2} + O(d_2^3, \delta_2^3)
\end{aligned} \tag{34}$$

where all the derivatives are computed at the arbitrary point C.

Substituting Eqs.(34) into (33c) and noting that $d \simeq u_1^C\bar{\delta}$, with $\bar{\delta} = (\delta_1 + \delta_2)$, $d_1 \simeq u_1^C\delta_1$ and $d_2 \simeq u_1^C\delta_2$ (Figure 3) and that the position of point C is arbitrary, gives the FIC equation for the free surface height (neglecting high order terms) as

$$r_\beta - \underline{\frac{h}{2}\frac{\partial r_\beta}{\partial x_1}} - \underline{\frac{\delta}{2}\frac{\partial r_\beta}{\partial t}} = 0 \tag{35}$$

with

$$r_\beta = \frac{\partial\beta}{\partial t} + u_1\frac{\partial\beta}{\partial x_1} - u_2 \tag{36}$$

where $h = (d_1 - d_2)$ and $\delta = (\delta_1 - \delta_2)$ are space and time stabilization parameters. The standard infinitesimal form of the free surface wave condition is obtained by making $h = \delta = 0$ in Eq.(35) giving

$$\frac{\partial\beta}{\partial t} + u_1\frac{\partial\beta}{\partial x_1} - u_2 = 0 \tag{37}$$

which coincides with equation (11) for the 2D case.

A simpler FIC expression can be derived from Eq.(35) by retaining the second order space term only. This gives

$$\frac{\partial\beta}{\partial t} + u_1\frac{\partial\beta}{\partial x_1} - \frac{u_1 h}{2}\frac{\partial^2\beta}{\partial x_1^2} - u_2 = 0 \tag{38}$$

This can be interpreted as the addition of an artificial diffusion term where $\frac{u_1 h}{2}$ plays the role of the new balancing diffusion coefficient.

In the following we will use the 3D ALE form of Eq.(35) neglecting the time stabilization term, given by

$$r_\beta - \underline{\frac{h_j}{2}\frac{\partial r_\beta}{\partial x_j}} = 0 \qquad \text{with} \quad r_\beta = \frac{\partial\beta}{\partial t} + v_j\frac{\partial\beta}{\partial x_j} - v_3 \quad , \quad j = 1, 2 \tag{39}$$

where v_i are the relative velocities between the fluid and the moving mesh nodes.

Encyclopedia of Computational Mechanics. Edited by Erwin Stein, René de Borst and Thomas J.R. Hughes.

6. FINITE ELEMENT DISCRETIZATION

6.1. Discretization of the fluid flow equations

We will choose C° continuous linear interpolations of the velocities, the pressure, the convection projections c_i and the pressure gradient projections π_i over three node triangles (2D) and four node tetrahedra (3D). The interpolations are written as

$$\begin{aligned} u_i &= \sum_{j=1}^{n} N_j \bar{u}_i^j \quad , \quad p = \sum_{j=1}^{n} N_j \bar{p}^j \\ c_i &= \sum_{j=1}^{n} N_j \bar{c}_i^j \quad , \quad \pi_i = \sum_{j=1}^{n} N_j \bar{\pi}_i^j \end{aligned} \tag{40}$$

where $n = 3$ (4) for triangles (tetrahedra), $\bar{(\cdot)}$ denotes nodal variables and N_j are the linear shape functions (Zienkiewicz and Taylor, Vol 1 2000).

Substituting the approximations (40) into Eqs.(32) and choosing the Galerking form with $\delta u_i = q = \delta c_i = \delta \pi_i = N_i$ leads to following system of discretized equations

$$\mathbf{M}\dot{\bar{\mathbf{u}}} + (\mathbf{A} + \mathbf{K} + \hat{\mathbf{K}})\bar{\mathbf{u}} - \mathbf{G}\bar{\mathbf{p}} + \mathbf{C}\bar{\mathbf{c}} = \mathbf{f} \tag{41a}$$

$$\mathbf{G}^T\bar{\mathbf{u}} + \mathbf{L}\bar{\mathbf{p}} + \mathbf{Q}\bar{\boldsymbol{\pi}} = \mathbf{0} \tag{41b}$$

$$\hat{\mathbf{C}}\bar{\mathbf{u}}_i + \mathbf{M}\bar{\mathbf{c}}_i = \mathbf{0} \quad , \quad i = 1, n_d \tag{41c}$$

$$\mathbf{Q}^T\bar{\mathbf{p}} + \hat{\mathbf{M}}\bar{\boldsymbol{\pi}} = \mathbf{0} \tag{41d}$$

The element contributions are given by (for 2D problems)

$$\begin{aligned} M_{ij} &= \int_{\Omega^e} \rho N_i N_j d\Omega \quad , \quad A_{ij} = \int_{\Omega^e} N_i \rho \mathbf{u}^T \nabla N_j d\Omega \quad , \quad \mathbf{K}_{ij} = \int_{\Omega^e} \mathbf{B}_i^T \mathbf{D} \mathbf{B}_j d\Omega \\ \hat{\mathbf{K}}_{ij} &= \int_{\Omega^e} \rho \frac{h_k u_l}{2} \frac{\partial N_i}{\partial x_k} \frac{\partial N_j}{\partial x_l} d\Omega \quad , \quad \mathbf{G}_{ij} = \int_{\Omega^e} (\nabla N_i) N_j d\Omega \quad , \quad \mathbf{C} = \int_{\Omega^e} \frac{h_k}{2} \frac{\partial N_i}{\partial x_k} N_j d\Omega \, d\Omega \\ L_{ij} &= \int_{\Omega^e} \nabla^T N_i [\tau] \nabla N_j d\Omega \; , \; \hat{\mathbf{C}}_{ij} = \int_{\Omega^e} N_i \rho u_k \frac{\partial N_j}{\partial x_k} d\Omega \; , \; \nabla = \left\{ \begin{array}{c} \dfrac{\partial}{\partial x_1} \\ \dfrac{\partial}{\partial x_2} \end{array} \right\} \; , \; [\tau] = \left[\begin{array}{cc} \tau_1 & 0 \\ 0 & \tau_2 \end{array} \right] \\ \mathbf{Q} &= [\mathbf{Q}^1, \mathbf{Q}^2] \quad , \quad Q_{ij}^k = \int_{\Omega^e} \tau_k \frac{\partial N_i}{\partial x_k} N_j d\Omega \\ \hat{\mathbf{M}} &= \left[\begin{array}{cc} \hat{\mathbf{M}}^1 & \mathbf{0} \\ \mathbf{0} & \hat{\mathbf{M}}^2 \end{array} \right] \quad , \quad \hat{\mathbf{M}}_{ij}^k = \int_{\Omega^e} \tau_k N_i N_j d\Omega \\ \mathbf{f}_i &= \int_{\Omega^e} N_i \mathbf{b} d\Omega + \int_{\Gamma^e} N_i \mathbf{t} d\Gamma \quad , \quad \mathbf{b} = [b_1, b_2]^T, \, \mathbf{t} = [t_1, t_2]^T \end{aligned} \tag{42}$$

with $i, j = 1, n$ and $k, l = 1, n_d$.

Encyclopedia of Computational Mechanics. Edited by Erwin Stein, René de Borst and Thomas J.R. Hughes.

In above $\mathbf{B}_i$ is the standard strain rate matrix and $\mathbf{D}$ the deviatoric constitutive matrix (for $\frac{\partial u_i}{\partial x_i} = 0$). For 2D problems

$$\mathbf{B}_i = \begin{bmatrix} \frac{\partial N_i}{\partial x_1} & 0 \\ 0 & \frac{\partial N_i}{\partial x_2} \\ \frac{\partial N_i}{\partial x_1} & \frac{\partial N_i}{\partial x_2} \end{bmatrix} \quad , \quad \mathbf{D} = \mu \begin{bmatrix} 2 & 0 & 0 \\ 0 & 2 & 0 \\ 0 & 0 & 1 \end{bmatrix} \tag{43}$$

In Eq.(42c) $\bar{\mathbf{u}}_i$ and $\bar{\mathbf{c}}_i$ contain the nodal degrees of freedom corresponding to the velocity component u_i and the convective projection c_i, respectively. Note that the stabilization matrix $\hat{\mathbf{K}}$ brings in an additional orthotropic diffusivity of value $\rho\frac{h_k u_l}{2}$. Matrices $\mathbf{A}, \hat{\mathbf{K}}$ and $\hat{\mathbf{C}}$ are dependent on the velocity field. The solution process can be advanced in time in a (quasi-nearly) implicit iterative manner using the following scheme.

Step 1

$$\bar{\mathbf{u}}^{n+1,i} = \bar{\mathbf{u}}^n - \Delta t \mathbf{M}^{-1}[(\mathbf{A}^{n+\theta_1,i-1} + \mathbf{K} + \hat{\mathbf{K}}^{n+\theta_1,i-1})\bar{\mathbf{u}}^{n+\theta_1,i-1} - \mathbf{G}\mathbf{p}^{n+\theta_2,i-1} + \mathbf{C}\bar{\mathbf{c}}^{n+\theta_3,i-1} - \mathbf{f}^{n+1}] \tag{44}$$

Step 2

$$\mathbf{p}^{n+1,i} = -\mathbf{L}^{-1}[\mathbf{G}^T\bar{\mathbf{u}}^{n+1,i} + \mathbf{Q}\bar{\pi}^{n+\theta_4,i-1}] \tag{45}$$

Step 3

$$\bar{\mathbf{c}}_j^{n+1,i} = -\mathbf{M}^{-1}\hat{\mathbf{C}}^{n+1,i}\bar{\mathbf{u}}_j^{n+1,i} \quad , \quad j = 1, n_d \tag{46}$$

Step 4

$$\bar{\boldsymbol{\pi}}^{n+1,i} = -\hat{\mathbf{M}}^{-1}\mathbf{Q}^T\bar{\mathbf{p}}^{n+1,i} \tag{47}$$

In above θ_i are time integration parameters with $0 \leq \theta_i \leq 1$ and $\bar{(\cdot)}^{n,i}$ denotes nodal values at the nth time step and the ith iteration. $\mathbf{A}^{n+\theta_1,i-1} \equiv \mathbf{A}(\bar{\mathbf{u}}^{n+\theta_1,i-1})$ etc. Also $(\cdot)^{n+\theta_i,0} \equiv (\cdot)^n$ for the computations in step 1 at the onset of the iterations.

Steps 1, 3 and 4 can be solved explicitely by choosing a *lumped (diagonal) form* of matrices $\mathbf{M}$ and $\hat{\mathbf{M}}$. In this manner the main computational cost is the solution of step 2 involving the inverse of a Laplacian matrix. This can be solved very effectively using an iterative method.

For $\theta_i \neq 0$ the iterative proces is unavoidable. The iterations follow until convergence is reached. This can be measured using an adequate error norm in terms of the velocity and pressure variables, or the residuals. Indeed some ot the θ_i's can be made equal to zero. Note that for $\theta_2 = 0$ the algorithm is inconditionable unstable. A simple semi-implicit form is obtained making $\theta_1 = \theta_3 = \theta_4 = 0$. Now all steps can be solved explicitely with exception of Step 2 for the pressure which still requires the solution of a simultaneous system of equations.

Convergence of this solution scheme is however difficult for some problems. An enhanced version of the algorithm can be obtained by simply adding the term $\hat{\mathbf{L}}(\bar{\mathbf{p}}^{n+1,i} - \bar{\mathbf{p}}^{n+1,i-1})$

Encyclopedia of Computational Mechanics. Edited by Erwin Stein, René de Borst and Thomas J.R. Hughes.

where $\hat{L}_{ij} = \Delta t \int_{\Omega^e} \boldsymbol{\nabla}^T N_i \boldsymbol{\nabla} N_j d\Omega$ to the equation for the computation of the pressure in the second step. The new term acts as a preconditioner of the pressure equation given now by

$$\bar{\mathbf{p}}^{n+1,i} = -[\mathbf{L} + \hat{\mathbf{L}}]^{-1}[\mathbf{G}^T \bar{\mathbf{u}}^{n+1,i} + \hat{\mathbf{L}}\bar{\mathbf{p}}^{n+1,i-1} + \mathbf{Q}\bar{\boldsymbol{\pi}}^{n+\theta_4,i-1}] \tag{48}$$

Note that the added term vanishes for the converged solution (i.e. when $\bar{\mathbf{p}}^{n+1,i} = \bar{\mathbf{p}}^{n+1,i-1}$).

An alternative to above algorithm is to use the fractional step method described in the nex section.

6.2. Fractional step method

The pressure can be split from the momentum equations as

$$\bar{\mathbf{u}}^* = \bar{\mathbf{u}}^n - \Delta t \mathbf{M}^{-1}[(\mathbf{A}^{n+\theta_1} + \mathbf{K} + \hat{\mathbf{K}}^{n+\theta_1})\bar{\mathbf{u}}^{n+\theta_1} - \alpha \mathbf{G}\bar{\mathbf{p}}^n + \mathbf{C}\bar{\mathbf{c}}^{n+\theta_3} - \mathbf{f}^{n+1}] \tag{49}$$

$$\bar{\mathbf{u}}^{n+1} = \bar{\mathbf{u}}^* + \Delta t \mathbf{M}^{-1}\mathbf{G}\delta\bar{\mathbf{p}} \tag{50}$$

In above equations α is a variable taking values equal to zero or one. For $\alpha = 0$, $\delta p \equiv p^{n+1}$ and for $\alpha = 1$, $\delta p = \Delta p$. Note that in both cases the sum of Eqs.(49) and (50) gives the time discretization of the momentum equations with the pressures computed at t^{n+1}. The value of $\bar{\mathbf{u}}^{n+1}$ from Eq.(50) is substituted now into (41b) to give

$$\mathbf{G}^T \bar{\mathbf{u}}^* + \Delta t \mathbf{G}^T \mathbf{M}^{-1}\mathbf{G}\delta\bar{\mathbf{p}} + \mathbf{L}\bar{\mathbf{p}}^{n+1} + \mathbf{Q}\bar{\boldsymbol{\pi}}^{n+\theta_4} = 0 \tag{51a}$$

The product $\mathbf{G}^T\mathbf{M}^{-1}\mathbf{G}$ can be approximated by a laplacian matrix, i.e.

$$\mathbf{G}^T\mathbf{M}^{-1}\mathbf{G} = \hat{\mathbf{L}} \quad \text{with } \hat{\mathbf{L}} \simeq \int_{\Omega^e} \frac{1}{\rho}(\nabla^T N_i)\nabla N_j \, d\Omega \tag{51b}$$

A semi-implicit algorithm can be derived as follows.

Step 1 Compute the nodal fractional velocities $\mathbf{u}^*$ explicitely from Eq.(49) with $\mathbf{M} = \mathbf{M}_d$ where subscript d denotes a diagonal matrix.

Step 2 Compute $\delta\bar{\mathbf{p}}$ from Eq.(51a) (using Eq.(51b)) as

$$\delta\bar{\mathbf{p}} = -(\mathbf{L} + \Delta t\hat{\mathbf{L}})^{-1}[\mathbf{G}^T\bar{\mathbf{u}}^* + \mathbf{Q}\bar{\boldsymbol{\pi}}^{n+\theta_4} + \mathbf{L}\bar{\mathbf{p}}^n] \tag{52}$$

Step 3 Compute the nodal velocities $\bar{\mathbf{u}}^{n+1}$ explicitely from Eq.(50) with $\mathbf{M} = \mathbf{M}_d$

Step 4 Compute $\bar{\mathbf{c}}^{n+1}$ explicitely from Eq.(46) using $\mathbf{M}_d$.

Step 5 Compute $\bar{\boldsymbol{\pi}}^{n+1}$ explicitely from Eq.(47) $\hat{\mathbf{M}} = \bar{\mathbf{M}}_d$.

This algorithm has an additional step from the iterative algorithm of Section 6.1. The advantage is that now Steps 1 and 2 can be fully linearized by choosing $\theta_1 = \theta_3 = \theta_4 = 0$. Also the equation for the pressure variables in Step 2 has improved stabilization properties due to the additional laplacian matrix $\hat{\mathbf{L}}$.

Details on the stability properties of the FIC formulation for incompressible fluid flow problems can be found in Oñate *et al.* (2002).

Encyclopedia of Computational Mechanics. Edited by Erwin Stein, René de Borst and Thomas J.R. Hughes.

6.3. Discretization of free surface wave equation

The solution in time of Eq.(39) can be written in terms of the nodal velocities computed from the flow solution, as

$$\beta^{n+1} = \beta^n - \Delta t \left[v_i^{n+1,i} \frac{\partial \beta^n}{\partial x_i} - v_3^{n+1,i} - \frac{h_{\beta_j}}{2} \frac{\partial r_\beta^n}{\partial x_j} \right] \tag{53}$$

Eq.(53) can now be discretized in space using the standard Galerkin method and solved *explicitely* for the nodal wave heights at t^{n+1}. Typically the general algorithm will be as follows:

1. Solve for the nodal velocities $\bar{\mathbf{u}}^{n+1}$ and the pressures $\bar{\mathbf{p}}^{n+1}$ in the fluid domain using any of the algorithms of Sections 6.1 and 6.2. When solving for the pressure equation impose $p^{n+1} = p_a$ at the free surface Γ_β.
2. Solve for the free surface elevation β^{n+1} (viz. Eq.(53)).
3. Compute the new position of the mesh nodes in the fluid domain at time t^{n+1}. Alternatively, regenerate a new mesh.

The mesh updating process can also include the free surface nodes, although this is not strictly necessary. An *hydrostatic adjustement* can be implemented once the new free surface elevation is computed simply by imposing the pressure at the nodes on the reference surface as

$$p^{n+1} = p_a + \rho |g| \Delta\beta \quad \text{with} \quad \Delta\beta = \beta^{n+1} - \beta^{\text{ref}} \tag{54}$$

Eq.(54) takes into account the changes in the free surface without the need of updating the reference surface nodes. A higher accuracy in the flow solution can be obtained by updating these nodes after a number of time steps.

7. FLUID-SHIP INTERACTION

The algorithms of previous section can be extended to account for the ship motion due to the sea forces. Here the ship hull structure can be modelled as a rigid solid defined by the three translations and the three rotations of its center of gravity. Alternatively, the full deformation of the ship structure can be computed by modelling the actual stiffness of the hull, the decks and the different structural members. Indeed, the former option usually suffices for the hull shape optimization.

In both cases the computation of the ship motion involves solving the dynamic equations of the ship structure written as

$$\mathbf{M}_s \ddot{\mathbf{d}} + \mathbf{K}_s \mathbf{d} = \mathbf{f}_{\text{ext}} \tag{55}$$

where $\mathbf{d}$ and $\ddot{\mathbf{d}}$ are the displacement and acceleration vectors of the nodes discretizing the ship structure, respectively, $\mathbf{M}_s$ and $\mathbf{K}_s$ are the mass and stiffness matrices of the structure and $\mathbf{f}_{\text{ext}}$ is the vector of external nodal forces accounting for the fluid flow loads induced by the pressure and the viscous stresses. Clearly the main driving forces for the motion of the ship is the fluid

Encyclopedia of Computational Mechanics. Edited by Erwin Stein, René de Borst and Thomas J.R. Hughes.

pressure which acts in the form of a surface traction. Indeed Eq.(55) can be augmented with an appropriate damping term. The form of all the relevant matrices and vectors can be found in standard books on FEM for structural analysis (Zienkiewicz and Taylor, Vol 2 2000).

Solution of Eq.(55) in time can be performed using implicit or fully explicit time integration algorithms. In both cases the values of the nodal displacements, the velocities and the accelerations at time t^{n+1} are found.

A typical coupled fluid-ship-structure solution in time using, for instance, the semi-implicit fractional step method of Section 2.2 involves the following steps.

Step 1 Solve for the fractional velocities $\bar{\mathbf{u}}^*$ using Eq.(49). Here use of $\alpha = 1$ is recommended.

Step 2 Compute $\delta\bar{\mathbf{p}}$ from Eq.(51a) solving a simultaneous system of equations.

Step 3 Compute explicitely the nodal velocities $\bar{\mathbf{u}}^{n+1}$ from Eq.(50) with a diagonal mass matrix.

Step 4 Compute explicitely the projected convective variables $\bar{\mathbf{c}}^{n+1}$ from Eq.(45) using $\mathbf{M}_d$.

Step 5 Compute explicitely the projected pressure gradients $\bar{\boldsymbol{\pi}}^{n+1}$ from Eq.(47) using $\hat{\mathbf{M}}_d$.

Step 6 Compute explicitely the new position of the free surface elevation $\bar{\boldsymbol{\beta}}^{n+1}$ from Eq.(53).

Step 7 Compute the movement of the ship by solving the dynamic equations of motion for the ship structure under the sea forces induced by the pressures $\bar{\mathbf{p}}^{n+1}$ and the viscous stresses $\mathbf{s}^{n+1}$.

Step 8 Update the position of the mesh nodes in the fluid domain at t^{n+1} by using the mesh update algorithm described next. The updating process can also include the free surface nodes at every time step, although this is not strictly necessary and the hydrostatic adjustment of the pressure acting on the free surface (Section 6.3) can be used as an alternative.

A cheaper option is to update the position of the mesh nodes once the iterative process for the fluid and solid variables has converged. Clearly the regeneration of the mesh is unavoidable when the distorsion of the element exceeds a certain limit.

8. A SIMPLE ALGORITHM FOR UPDATING THE MESH NODES

Different techniques have been proposed for dealing with mesh updating in fluid-structure interaction problems. The general aim of all methods is to prevent element distortion during mesh deformation (Tezduyar, 2001; Tezduyar *et al.*, 1992a, 1992b).

Chiandussi *et al.* (2000) have proposed a simple method for moving the mesh nodes based on the iterative solution of a fictious linear elastic problem on the mesh domain. In order to minimize the mesh deformation the "elastic" properties of each mesh element are appropiately selected so that elements suffering greater movements are stiffer. A simple and effective procedure is to select the Poisson's ratio $\nu = 0$ and compute the "equivalent" Young modulus

Encyclopedia of Computational Mechanics. Edited by Erwin Stein, René de Borst and Thomas J.R. Hughes.

for each element by

$$E = \frac{\bar{E}}{3\bar{\varepsilon}^2}(\varepsilon_1^2 + \varepsilon_2^2 + \varepsilon_3^2) \tag{56}$$

where ε_i are the principal strains, $\bar{E}$ is an arbitrary value of the Young modulus and $\bar{\varepsilon}$ is a prescribed uniform strain field. $\bar{E}$ and $\bar{\varepsilon}$ are constant for all the elements in the mesh.

The solution process includes the following two steps.

Step 1. Consider the FE mesh as a linear elastic solid with homogeneous material properties characterized by a prescribed uniform strain field $\bar{\varepsilon}$, an arbitrary Young modulus E and $\nu = 0$. Solve a linear elastic problem with imposed displacements at the mesh boundary defined by the actual movement of the boundary nodes.

Step 2. Compute the principal strains in each element. Repeat the FE solution of the linear elastic problem with prescribed boundary displacements using the values of E of Eq.(56).

The previous algorithm is able to treat the movement of the mesh due to changes in position of fully submerged and semi-submerged bodies such as ships. However if the floating body intersects the free surface, the changes in the analysis domain can be very important as emersion or inmersion of significant parts of the body can occur within a time step. A possible solution to this problem is to remesh the analysis domain. However, for most problems a mapping of the moving surfaces linked to mesh updating algorithm described above can avoid remeshing. The surface mapping technique used by the authors is based on transforming the 3D curved surfaces into reference planes (Figure 4). This makes it possible to compute within each plane the local (in-plane) coordinates of the nodes for the final surface mesh accordingly to the changes in the floating line. The final step is to transform back the local coordinates of the surface mesh in the reference plane to the final curved configuration which incorporates the new floating line (García, 1999; Oñate and García, 2001).

9. MODELLING OF THE TRANSOM STERN FLOW

The transom stern causes a discontinuity in the domain and the solution of the free surface equation close to this region is inconsistent with the convective nature of the equation. This leads to instability of the wave height close to the transom region. This instability is found experimentally for low speeds. The flow at a sufficient high speed is physically more stable although it still can not be reproduced by standard numerical techniques (Reed *et al.*, 1990).

A solution to this problem is to apply adequate free surface boundary conditions at the transom boundary. The obvious condition is to fix both the free surface elevation β and its derivative along the corresponding streamline to values given by the transom position and the surface gradient. However, prescribing those values can influence the transition between the transom flux and the lateral flux, resulting in unaccurate wave maps.

The method proposed in García and Oñate (2002) is to extend the free surface below the ship. In this way the necessary Dirichlet boundary conditions imposed at the inflow domain are enough to define a well posed problem. This method is valid both for the wetted and dry transom cases and it can be also applied to ships with regular stern.

This scheme does not work for partially wetted transoms. This situation can occur for highly unsteady flows where wake vortex induces the free surface deformation and the flow remains

Encyclopedia of Computational Mechanics. Edited by Erwin Stein, René de Borst and Thomas J.R. Hughes.

adhered to the transom. To favour the convergence of the free surface, an artificial viscosity term is added to the free surface equation in the vecinity of the transom in these cases.

10. LAGRANGIAN FLOW FORMULATION

The lagrangian formulation is an effective (and relatively simple) procedure for modelling the flow of fluid particles undergoing severe distorsions such as water jets, high amplitude waves, braking waves, water splashing, filling of cavities, etc. Indeed the lagrangian formulation is very suitable for treating ship hydrodynamic problems where the ship undergoes large motions. An obvious "a priori" advantage of the lagrangian formulation is that both the ship and the fluid motion are defined in the same frame of reference.

The lagrangian fluid flow equations are obtained by noting that the velocity of the mesh nodes and that of the fluid particles are the same. Hence the relative velocities v_i are zero in Eq.(21) and the convective terms vanish in the momentum equations, while the rest of the fluid flow equations remain unchanged.

The FEM algorithms for solving the lagrangian flow equations are very similar to those for the ALE description presented earlier here. We will focus in the semi-implicit fractional step algorithm of Section 6.2 (for $\theta_1 = \theta_4 = 0$ and $\alpha = 1$) accounting also for fluid-structure interaction effects.

Step 1 Compute explicitely a predicted value of the velocities $\mathbf{u}^*$ as

$$\bar{\mathbf{u}}^* = \bar{\mathbf{u}}^n - \Delta t \mathbf{M}_d^{-1}[\mathbf{K}\bar{\mathbf{u}}^n - \mathbf{G}\bar{\mathbf{p}}^n - \mathbf{f}^{n+1}] \tag{57}$$

Note that the convective matrices $\mathbf{A}$ and $\bar{\mathbf{K}}$ of Eq.(48)have been elliminated.

Step 2 Compute $\delta\bar{\mathbf{p}}$ from Eq.(52).

Step 3 Compute explicitely $\bar{\mathbf{u}}^{n+1}$ from Eq.(50) with $\mathbf{M} = \mathbf{M}_d$.

Step 4 Compute $\bar{\boldsymbol{\pi}}^{n+1}$ explicitely from Eq.(46).

Step 5 Solve for the motion of the structure by integrating Eq.(55).

Step 6 Update the mesh nodes in a lagrangian manner as

$$\mathbf{x}_i^{n+1} = \mathbf{x}_i^n + \bar{\mathbf{u}}_i \Delta t \tag{58}$$

Step 7 Generate a new mesh.

The mesh regeneration process can be effectively performed using the extended Delaunay Tesselation described in Idelsohn *et al.* (2002a). This method allows the fast generation of good quality meshes combining four node tetrahedra (or three node triangles in 2D) with non standard polyedra such as pentahedra (or pentagons in 2D) where linear shape functions are derived using non-Sibsonian interpolation rules. The mesh regeneration can take place after a prescribed number of time steps, or when the nodal displacements induce significant element distorsions.

Encyclopedia of Computational Mechanics. Edited by Erwin Stein, René de Borst and Thomas J.R. Hughes.

The identification of the free surface nodes in the lagrangian analysis can be made using the Alpha Shape method. This is based on the search of all nodes which are on an empty Voronoi sphere with a radius greater than a specified distance defined in terms of the discretization size. For details see Edelsbrunner and Mucke (1994) and Idelsohn *et al.* (2002b,c).

The boundary conditions of prescribed velocities or pressures in the lagrangian formulation are usually applied on a layer of nodes adjacent to the boundary. These nodes typically remain fixed during the solution process. For details see Idelsohn *et al.* (2002b,c).

11. COMPUTATION OF THE CHARACTERISTIC LENGTHS

The evaluation of the stabilization parameters is a crucial issue in stabilized methods. Most of existing methods use expressions which are direct extensions of the values obtained for the simplest 1D case. It is also usual to accept the so called SUPG assumption, i.e. to admit that vector $\mathbf{h}$ has the direction of the velocity field. This restriction leads to instabilities when sharp layers transversal to the velocity direction are present. This deficiency is usually corrected by adding a shock capturing or crosswind stabilization term (Hughes and Mallet, 1986; Codina, 1993). Indeed, in the FIC formulation the components of $\mathbf{h}$ introduce the necessary stabilization along both the streamline and transversal directions to the flow.

Excellent results have been obtained in all problems solved using linear tetrahedra with the value of the characteristic length vector defined by

$$\mathbf{h} = h_s \frac{\mathbf{u}}{u} + h_c \frac{\nabla u}{|\nabla u|} \tag{59}$$

where $u = |\mathbf{u}|$ and h_s and h_c are the "streamline" and "cross wind" contributions given by

$$h_s = \max(\mathbf{l}_j^T \mathbf{u})/u \tag{60}$$

$$h_c = \max(\mathbf{l}_j^T \nabla u)/|\nabla u| \quad , \quad j = 1, n_s \tag{61}$$

where $\mathbf{l}_j$ are the vectors defining the element sides ($n_s = 6$ for tetrahedra).

As for the free surface equation the following value of the characteristic length vector $\mathbf{h}_\beta$ has been taken

$$\mathbf{h}_\beta = \bar{h}_s \frac{\mathbf{u}}{u} + \bar{h}_c \frac{\nabla \beta}{|\nabla \beta|} \tag{62}$$

The streamline parameter $\bar{h}_s$ has been obtained by Eq.(60) using the value of the velocity vector $\mathbf{u}$ over the 3 node triangles discretizing the free surface and $n_s = 3$.

The cross wind parameter $\bar{h}_c$ has been computed by

$$\bar{h}_c = \max[\mathbf{l}_j^T \nabla \beta] \frac{1}{|\nabla \beta|} \quad , \quad j = 1, 2, 3 \tag{63}$$

The cross-wind terms in eqs.(59) and (62) take into account the gradient of the solution in the stabilization parameters. This is a standard assumption in shock-capturing stabilization procedures.

A more consistent evaluation of $\mathbf{h}$ based on a diminishing residual technique can be found in Oñate and García (2001).

Encyclopedia of Computational Mechanics. Edited by Erwin Stein, René de Borst and Thomas J.R. Hughes.

12. TURBULENCE MODELLING

The detailed discussion on the treatment of turbulent effects in the flow equations falls outside the scope of this chapter. Indeed any of the existing turbulence models is applicable.

In the examples presented next we have chosen a turbulence model based on the Reynolds averaged Navier-Stokes equations where the deviatoric stresses are computed as sum of the standard viscous contributions and the so called Reynold stresses. Here we have chosen the Boussinesq assumption leading to a modification of the viscosity in the standard Navier-Stokes equations as sum of the "physical" viscosity μ and a turbulent viscosity μ_T.

One of the simplest and more effective choices for μ_T is the Smagorinski LES model giving

$$\mu_T = C_l h^e (2\varepsilon_{ij}\varepsilon_{ij})^{1/2} \tag{64}$$

where h^e is the element size and C is a constant ($C \simeq 0.01$).

Many other options are possible such as the one and two equations turbulence models (i.e. the k model and the $k-\varepsilon$ and $k-w$ models) and the algebraic stress models. For further details the reader is refered to specialized publications (Celik *el al.*, 1982; Wilcox, 1994).

13. EXAMPLES

The examples chosen show the applicability of the ALE and lagrangian formulations presented to solve ship hydrodynamics problems. The fractional step algorithm of Section 6.2 with $\theta_1 = \theta_3 = \theta_4 = 0$ and $\alpha = 1$ has been used. The first ALE example is the flow past a submerged NACA 0012 profile. The next ALE examples include the analysis of a Wigley hull, a scale model of a commercial ship and two American Cup racing sail boats. Numerical results obtained with linear tetrahedral meshes are compared with experimental data in all cases.

The last series of examples show applications of the Lagrangian formulation to simple schematic 2D ship hydrodynamics situations.

13.1. Submerged NACA 0012 profile

A submerged NACA0012 profile at $\alpha = 5°$ angle of attack is studied using a 3D finite element model. This configuration was tested experimentally by Duncan (1983) and modelled numerically using the Euler equations by several authors (Hino *et al.*, 1993; Löhner *et al.*, 1996; Idelsohn *et al.*, 1999). The submerged depth of the airfoil is equal to the chord length L. The Froude number for all the cases tested was set to $Fr = \frac{U}{\sqrt{gL}} = 0.5672$ where U is the incoming flow velocity at infinity.

The stationary free surface and the pressure distribution in the domain are shown in Figure 5. The non-dimensional wave heights compare well with the experimental results.

13.2. Wigley hull

We study here the well known Wigley Hull, given by the analytical formula $y = 0.5B(1 - 4x^2)(1 - z^2/D^2)$ where B and D are the beam and the draft of the ship hull at still water.

The same configuration was tested experimentally (Noblesse and McCarthy, 1983; Wigley, 1983) and modelled numerically by several authors (Farmer *et al.*, 1993; Storti *et al.*, 1998;

Encyclopedia of Computational Mechanics. Edited by Erwin Stein, René de Borst and Thomas J.R. Hughes.

Idelsohn *et al.*, 1999; Löhner *et al.*, 1999). We use an unstructured 3D finite element mesh of 65434 linear tetrahedra, with a reference surface of 7800 triangles, partially represented in Figure 6. A Smagorinsky turbulence model was chosen.

Three different viscous cases were studied for $L = 6m, F_n = 0.316, \mu = 10^{-3} Kg/m.s$. In the first case the volume mesh was considered fixed, not allowing free surface nor ship movements. Next, the volume mesh was updated due to free surface movement, while keeping the model fixed. The third case corresponds to the analysis of a real free model including the mesh updating due to free surface displacement and ship movement (sinkage and trim).

Table 1 shows the obtained total resistance coefficient in the three cases studied compared with experimental data.

	Experimental	**Numerical**
Test 1	$5.2\ 10^{-3}$	$4.9\ 10^{-3}$
Test 2	$5.2\ 10^{-3}$	$5.3\ 10^{-3}$
Test 3	$4.9\ 10^{-3}$	$5.1\ 10^{-3}$

Table I. Wigley Hull. Total resistance coefficient values

Numerical values obtained for sinkage and trim were -0.1% and 0.035, respectively, while experiments gave -0.15% and 0.04.

Figure 6a shows the pressure distribution obtained near the Wigley hull for the free model. Some streamlines have also been plotted. The mesh deformation in this case is shown in Figure 6a.

Comparison of the obtained body wave profile with experimental data for the free and fixed models is shown in Figure 6b. Significant differences are found close to stern for the fixed model. The free surface contours for the truly free ship motion are shown in Figure 6c.

13.3. KVLCC2 hull model

The example is the analysis of the KVLCC2 benchmark model. Here a partially wetted tramsom stern is expected due to the low Froude number of the test. Figure 7 shows the NURBS geometry obtained from the Hydrodynamic Performance Research team of Korea (KRISO). Numerical results are compared with the experimental data available in KRISO (2000).

The smallest element size used was 0.001 m and the largest 0.50 m. The surface mesh chosen is also shown in Figure 7. The 3D mesh included 550.000 tetrahedra. The tramsom stern flow model described was used.

Test 1.- Wave pattern calculation. The main characteristics of the analysis are listed below:

- Length: 5.52 m, Beam (at water plane): 0.82 m, Draught: 0.18 m, Wetted Surface: $8.08m^2$.
- Velocity: 1.05 m/seg, Froude Number: 0.142.
- Viscosity: $0.00126Kg/mseg$, Density: $1000Kg/m^3$, Reynolds number: 4.6310^6.

The turbulence model chosen was the K model. Figures 8 and 9 show the wave profiles on the hull and in a cut at y/L = 0.0964 obtained for Test 1, compared to experimental data. The results are quantitatively good.

Encyclopedia of Computational Mechanics. Edited by Erwin Stein, René de Borst and Thomas J.R. Hughes.

Test 2.- Wake analysis at different planes. Several turbulence models were used (*Smagorinsky*, K and $K-\epsilon$ model) in order to verify the quality of the results. Here, only the results from the $K-\epsilon$ model are shown. The velocity maps obtained even for the simplest *Smagorinsky* model were qualitatively good. The main characteristics of this analysis are:

- Length: 2.76 m, Beam (at water plane): 0.41 m, Draught: 0.09 m, Wetted Surface: $2.02m^2$.
- Velocity: 25 m/seg.
- Viscosity: $3.0510^{-5}Kg/mseg$, Density: $1.01Kg/m^3$, Reynolds number: 4.6310^6.

Figures 10 and 11 present some results for Test 2. Figure 10 shows the contours of the axial (X) component of the velocity on a plane at 2.71 m from the orthogonal aft. Figure 11 shows the map of the kinetic energy at this plane. Experimental results are also plotted for comparison. Further results are reported in García and Oñate (2000).

13.4. American Cup Rioja de España Model

The Rioja de España boat representing Spain in the American Cup's edition of 1995 was analyzed. Figure 12 shows the geometry of the boat based on standard NURBS surfaces. Numerical results are compared with an extrapolation of experimental data obtained in CEHIPAR basin (Spain) using a 1/3.5 scale model. Resistance tests were performed with the model free to sink and trim. Experimental data include drag, lift, sinkage, trim angles and wave profiles at 4.27m (real scale) from symmetry plane. Every model was towed at equivalent velocities of 10, 9, 8.5, 8.0, 7.5 and 7.0 knots.

Numerical analysis were carried out at real scale. Characteristics of unstructured grids of four node linear tetrahedra used are shown in Table 2 together with the parameters of some of the model studied.

Test	Geometry	Heel	Drift	Symmetry	# Elements	# nodes
E0D0	Hull, bulb and keel	0°	0°	Yes	700 000	175 000
E15D2	Hull, bulb, keel and rudder	15°	2°	No	1 500 000	380 000
E15D4	Hull, bulb, keel and rudder	15°	4°	No	1 500 000	380 000
E25D2	Hull, bulb, keel and rudder	25°	2°	No	1 500 000	380 000

Table II. Rioja de España. Analysis parameters.

All grids used were generated with the same quality criteria and using element sizes from 5mm to 2000 mm. Some details of the grid used in the E0D0 case are shown in Figures 13 and 14. A $k-\varepsilon$ turbulence model in combination with an extended law of the wall was chosen for the analysis.

A time step of 0.1 seconds was used and this sufficed to achieve a steady state solution in all cases. Additional calculations were carried out with $\Delta t = 0.025s$ and $0.01s$, in order to verify the influence of the time increment in the accuracy of the results. No significant influence was detected for the selected results.

Figure 16 shows a comparison of simulated and experimental wave profiles. The origin of the x axis has been taken at the fore perpendicular and the x+ sense is afore. In the non symmetric case, the measurements were performed at the opposite side of the heeled board. The ratio of maximum amplitudes of fluctuations (noise) and waves in the experimental measurements varies from 4% to 12%.

Encyclopedia of Computational Mechanics. Edited by Erwin Stein, René de Borst and Thomas J.R. Hughes.

Figures 16 and 17 show pressure contours on the bulb and keel for different cases, corresponding to a velocity of 8 kn. Figures 18 to 19 show some of the wave patterns obtained for a velocity of 9 kn. Figures 21 and 22 show some perspective views, including pressure and velocity contours, streamlines and cuts, for some cases analyzed. Finally Figures 23 and 24 show resistance graphs where numerical results are compared with values extrapolated from experimental data. For further details see García *et al.* (2002).

13.5. American Cup BRAVO ESPAÑA Model

The finite element formulation presented was also applied to study the racing sail boat *Bravo España* participating in the 1999 edition of the American Cup. The mesh of linear tetrahedra used is shown in Figure 25. Results presented in Figures 25–27 correspond to a non symmetrical case including appendages. Good comparison between experimental data and numerical results was again obtained Further details can be found in García and Oñate (2002).

13.6. Lagrangian flow examples

A number of simple problems have been designed and solved in order to test the capabilities of the lagrangian flow formulation to solve ship hydrodynamics problem.

The first example is a very schematic representation of a ship when it is hit by a big wave produced by the collapse of a water recipient (Fig. 28). The ship cannot move and initially the free surface is horizontal. Fixed nodes represent the ship as well as the domain walls. The example tests the suitability of the lagrangian flow formulation to solve contact problems with curved walls correctly. Note the crash of the waves under the ship prow and the rebound of the wave. It is also interesting to see the different contact situations with the internal and external ship surfaces and the moving free surface at the bottom and back of the ship.

In the next example (Fig. 29) the same ship of the previous example is now moving horizontally at a fixed velocity. All the nodes representing the ship have a prescribed velocity. The free surface, which was initially horizontal, takes a correct position at the bottom of the ship. Again, the correct contact problem is realistically solved in the curved prow.

The last example shows an initially stationary recipient with a floating piece of wood where a wave is produced on the left side. The wood has been simulated by a liquid of higher viscosity. The wave intercepts the wood piece producing a breaking wave and displacing the floating wood as shown in Figure 30.

Further examples of the lagrangian flow formulation can be found in Idelsohn *et al.* (2002a,b).

14. CONCLUDING REMARKS

An overview of different finite element schemes for solving ship hydrodynamics problems has been presented. The necessary stabilization in the numerical computation has been provided by the finite calculus formulation of the fluid flow equations accounting for surface wave effects.

Stabilized finite algorithms for solving a variety of ship hydrodynamics situations using ALE and fully lagrangian descriptions have been presented. Both monolithic and fractional step algorithms have been derived. The interaction of the motion of the ship structure with the fluid equations can be accounted for in a straight forward manner within the general flow solution schemes. The ALE formulation is particularly adequate for ship hydrodynamics

Encyclopedia of Computational Mechanics. Edited by Erwin Stein, René de Borst and Thomas J.R. Hughes.

problems involving free surface waves of moderate amplitude. The lagrangian description allows to solve in an effective manner ship hydrodynamics problems involving large motions of the free surface and complex fluid-structure interaction situations.

ACKNOWLEDGEMENTS

The authors thank Prof. R. Löhner, Dr. C. Sacco and Dr. H. Sierra for many useful discussions.

The authors are also grateful to Copa America Desafio Español SA and CEHIPAR for providing the geometry and experimental data of the racing boats analyzed.

The Spanish company COMPASS Ingeniería y Sistemas SA (www.compassis.com) provided the computer code Tdyn for the numerical simulation of the examples solved with the ALE formulation (Tdyn, 2002). This support is gratefully acknowledged.

REFERENCES

Alessandrini B and Delhommeau G. A Fully Coupled Navier-Stokes Solver for Calculation of Turbulent Incompressible Free Surface Flow Past a Ship Hull. *J. Numer. Meth. Fluids* 1999; **29**:125–142.

Alessandrini B and Delhommeau G. A multigrid velocity-pressure-free surface elevation fully coupled solver for calculation of turbulent incompressible flow around a hull. In *Proc. of the 21st Symp. on Naval Hydrodynamics*, Trondheim, Norway, 1996, 40–55.

Aliabadi S and Shujaee S. Free surface flow simulations using parallel finite element method. *Simulation* 2001; **76(5)**:257–262.

Aliabadi S, Abedi J and Zellars B. Parallel finite element simulation of mooring forces on floating objects. Submitted to *Int. J. Num. Meth. Fluids* 2002.

Baba E and Takekuma K. A study on free-surface flow around bow of slowly moving full forms. *J. Soc. Naval Architects Japan* 1975; **137**.

Bai KJ and McCarthy JH (eds). *Proceedings of the Workshop on Ship Wave-Resistance Computations*, Bethesda, MD, USA, 1979.

Brezzi F, Franca LP, Hughes TJR and Russo A. $b = \int g$. *Comput. Methods Appl. Mech. Engrg.* 1997; **145**:329–339.

Briley WR, Neerarambam SS and Whitfield DL. Multigrid algorithm for three-dimensional incompressible high-Reynolds number turbulent flows. *AIAA Journal* 1995; **33 (1)**:2073–2079.

Brooks A and Hughes TJR. Streamline upwind/Petrov-Galerkin formulation for convection dominated flows with particular emphasis on the incompressible Navier-Stokes equations. *Comput. Methods Appl. Mech. Engrg* 1982; **32**:199–259.

Celik I; Rodi W and Hossain MS. Modelling of free surface proximity effects on turbulence. *Proc. Refined Modelling of Flows*, Paris, 1982.

Chiandusi G, Bugeda G and Oñate E. A simple method for update of finite element meshes. *Commun, Numer. Meth. Engng.* 2000; **16**:1–9.

Chorin AJ. A numerical solution for solving incompressible viscous flow problems. *J. Comp. Phys.* 1967; **2**:12–26.

Codina R. A discontinuity-capturing crosswind dissipation for the finite element solution of the convection-diffusion equation. *Comput. Methods Appl. Mech. Engrg.* 1993; **110**:325–342.

Codina R and Blasco J. A finite element formulation for the Stokes problem allowing equal velocity - pressure interpolation. *Comput. Methods Appl. Mech. Engrg.* 1997; **143**:373–391.

Codina R, Vazquez M, Zienkiewicz OC. A general algorithm for compressible and incompressible flow - Part III. The semi-implicit form. *Int. J. Num. Meth. in Fluids* 1998; **27**:13–32.

Encyclopedia of Computational Mechanics. Edited by Erwin Stein, René de Borst and Thomas J.R. Hughes.

Codina R. Comparison of some finite element methods for solving the diffusion-convection-reaction equation. *Comput. Methods Appl. Mech. Engrg.* 1998; **156**:185–210.

Codina R. A stabilized finite element method for generalized stationary incompressible flows. Publication PI-148, CIMNE, Barcelona, February 1999.

Codina R. On stabilized finite element methods for linear systems of convection-diffusion-reaction equation. *Comput. Methods Appl. Mech. Engrg.* 2000; **188**:61–83.

Codina R. Stabilization of incompressibility and convection through orthogonal sub-scales in finite element methods. *Comput. Methods Appl. Mech. Engrg.* 2000; **191**:4295–4321.

Codina R and Blasco J. Stabilized finite element method for the transient Navier-Stokes equations based on a pressure gradient operator. *Comput. Methods in Appl. Mech. Engrg.* 2000; **182**:277–301.

R. Codina, "Stabilized finite element approximation of transient incompressible flows using orthogonal subscales", *Comput. Methods Appl. Mech. Engrg.*, **191**, 4295–4321, 2002.

R. Codina and O.C. Zienkiewicz, "CBS versus GLS stabilization of the incompressible Navier-Stokes equations and the role of the time step as stabilization parameter", *Communications in Numerical Methods in Engineering*, **18 (2)**, 99–112, 2002.

Cruchaga MA and Oñate E. A finite element formulation for incompressible flow problems using a generalized streamline operator. *Comput. Methods in Appl. Mech. Engrg.* 1997; **143**:49–67.

Cruchaga MA and Oñate E. A generalized streamline finite element approach for the analysis of incompressible flow problems including moving surfaces. *Comput. Methods in Appl. Mech. Engrg.* 1999; **173**:241–255.

Dawson CW. A practical computer method for solving ship-wave problems. *Proc. 2nd Int. Conf. Num. Ship Hydrodynamics*, USA, 1977.

Donea J. A Taylor-Galerkin method for convective transport problems. *Int. J. Num. Meth. Engng.* 1984; **20**:101–119.

Douglas J, Russell TF. Numerical methods for convection dominated diffusion problems based on combining the method of characteristics with finite element or finite difference procedures. *SIAM J. Numer. Anal.* 1982; **19**:871.

Duncan JH. The breaking and non-breaking wave resistance of a two-dimensional hydrofoil. *J. Fluid Mech.* 1983; **126**.

Edelsbrunner H and Mucke EP. Three dimensional alpha-shape. *ACM Transaction on Graphics* 1994; **3**:43–72.

Farmer JR, Martinelli L and Jameson A. A fast multigrid method for solving incompressible hydrodynamic problems with free surfaces. *AIAA J.* 1993; **32 (6)**:1175–1182.

García J, Oñate E, Sierra H, Sacco C and Idelsohn SR. A stabilized numerical method for analysis of ship hydrodynamics. *ECCOMAS CFD98*, Papaliou K *et al.* (Eds), J. Wiley, 1998.

García J. A finite element method for analysis of naval structures (in Spanish). *Ph.D. Thesis*, Univ. Politècnica de Catalunya, Barcelona, Spain, December, 1999.

García J and Oñate E. An unstructured finite element solver for ship hydrodynamic problems. Accepted for publication in *J. Appl. Mech.*, 2002.

García J, Luco-Salman R, Salas M, López-Rodríguez M and Oñate E. An advanced finite element method for fluid-dynamic analysis of America's Cup boat. *High Performance Yatch Design Conference*, Auckland, 4–6, December, 2002.

Hansbo P and Szepessy A. A velocity-pressure streamline diffusion finite element method for the incompressible Navier-Stokes equations. *Comput. Methods Appl. Mech. Engrg.* 1990; **84**:175–192.

Hino T, Martinelli L and Jameson A. A finite volumen method with unstructured grid for free surface flow. In *Proc. of the 6th Int. Conf.Num. Ship Hydrodynamics*, Iowa City, Iowa, 1993, 173–194.

Encyclopedia of Computational Mechanics. Edited by Erwin Stein, René de Borst and Thomas J.R. Hughes.

Hirsch C. *Numerical computation of internal and external flow*, J. Wiley, Vol. 1 1988, Vol. 2, 1990.

Hirt CW and Nichols BD. Volume of fluid (VOF) method for the dynamics of free boundaries. *J. Comput. Physics* 1981; **39**:201–225.

Hughes TJR, Franca LP and Balestra M. A new finite element formulation for computational fluid dynamics. V Circumventing the Babuska-Brezzi condition: A stable Petrov-Galerkin formulation of the Stokes problem accomodating equal order interpolations. *Comput. Methods Appl. Mech. Engrg.* 1986; **59**:85–89.

Hughes TJR and Mallet M. A new finite element formulations for computational fluid dynamics: III. The generalized streamline operator for multidimensional advective-diffusive systems. *Comput Methods Appl. Mech. Engrg.* 1986; **58**:305–328.

Hughes TJR and Mallet M. A new finite element formulations for computational fluid dynamics: IV. A discontinuity capturing operator for multidimensional advective-diffusive system. *Comput. Methods Appl. Mech. Engrg.* 1986; **58**:329–336.

Hughes TJR, Franca LP and Hulbert GM. A new finite element formulation for computational fluid dynamics: VIII. The Galerkin/least-squares method for advective-diffusive equations. *Comput. Methods Appl. Mech. Engrg.* 1989; **73**:173–189.

Hughes TJR. Multiscale phenomena: Green functions, subgrid scale models, bubbles and the origins of stabilized methods. *Comput. Methods Appl. Mech. Engrg* 1995; **127**:387–401.

Idelsohn SR, Storti M and Nigro N. Stability analysis of mixed finite element formulation with special mention to stabilized equal-order interpolations. *Int. J. for Num. Meth. in Fluids* 1995; **20**:1003-1022.

Idelsohn SR, Oñate E and Sacco C. Finite element solution of free surface ship-wave problem. *Int. J. Num. Meth. Engng.* 1999; **45**:503–508.

Idelsohn SR, Oñate E, Calvo N and Del Pin F. The meshless finite element method. Accepted in *Int. J. Num. Meth. Engng*, 2002.

Idelsohn SR, Oñate E, Del Pin F and Calvo N. Lagrangian formulation: the only way to solve some free-surface fluid mechanics problems. *Fith World Congress on Computational Mechanics*, Mang HA, Rammerstorfer FG and Eberhardsteiner J. (eds), July 7–12, Viena, Austria, 2002, Web: wccm.tuwien.ac.at.

Idelsohn SR, Oñate E and Del Pin F. A lagrangian meshless finite element method applied to fluid-structure interaction problems. Submitted to *Computer and Structures*, 2002.

Janson C and Larsson L. A method for the optimization of ship hulls from a resistance point of view. *Proc. of the 21th Symp. on Naval Hidrodynamics*, Trondheim, Norway, 1996.

Jenson G and Soding H. Ship wave resistance computation. *Finite Approximations in Fluid Mechanics* 1989; **II**, Vol.**25**.

Kim YH and Lucas T. Nonlinear ship waves. *Proc. 18th Symp. on Naval Hidrodynamics*, MI, USA, 1990.

KRISO (Korea Research Institute of Ships and Ocean Engineering). http://www.iihr.uiowa.edu/gothenburg2000/KVLCC/tanker.html.

Larsson L. Procedings of the *1980 SSPA-ITTC Workshop on Ship Boundary Layers*. SSPA Publication No. 90, 1981.

Larsson L, Regnström B, Broberg L, Li DQ and Janson CE. Failures, fantasies and feats in the theoretical/numerical prediction of ship performance. *22d Symposium on Naval Hydrodynamics*, Washington DC, 10–14, August, 1998.

Löhner R., Morgan K, Zienkiewicz OC. The solution of non-linear hyperbolic equation systems by the finite element method. *Int. J. Num. Meth. in Fluids* 1984; **4**:1043.

Löhner R, Yang C, Oñate E and Idelsohn SR. An unstructured grid-based parallel free surface solver. *Appl. Num. Math.* 1999; **31**:271–293.

Encyclopedia of Computational Mechanics. Edited by Erwin Stein, René de Borst and Thomas J.R. Hughes.

Luo H, Baum JD and Löhner R. A finite volume scheme for hydrodynamic free boundary problems on unstructured grids. *AIAA*-95-0668, 1995.

Miyata H. Time-marching CFD simulation for moving boundary problems. In *Proc. of the 21st Symp. on Naval Hydrodynamics*, Trondheim, Norway, 1996, 1–21.

Nakos DE and Sclavounos PD. On steady and unsteady ship wave patterns. *J. of Fluid Mechanics* 1990; **215**:256–288.

Newman JN. Linearized wave resistance theory. *Int. Seminar on Wave Resistance*, Tokyo/Osaka, J. Soc. Naval Architects Japan, 1976.

Noblesse F and McCarthy JH (eds). *Proceedings of the Second DTNSRDC Workshop on Ship Wave-Resistance Computations*, Bethesda, MD, USA, 1983.

Oñate E and Idelsohn SR. A mesh free finite point method for advective-diffusive transport and fluid flow problems. *Computational Mechanics* 1988; **21**:283–292.

Oñate E, García J and Idelsohn SR. Computation of the stabilization parameter for the finite element solution of advective-diffusive problems. *Int. J. Num. Meth. Fluids* 1997; **25**:1385–1407.

Oñate E. Derivation of stabilized equations for advective-diffusive transport and fluid flow problems. *Comput. Methods Appl. Mech. Engrg.* 1998; **151 (1-2)**:233–267.

Oñate E, García J and Idelsohn SR. An alpha-adaptive approach for stabilized finite element solution of advective-diffusive problems with sharp gradients. *New Adv. in Adaptive Comput. Methods in Mech.*, Ladeveze P and Oden JT (eds), Elsevier, 1998.

Oñate E and Manzan M. A general procedure for deriving stabilized space-time finite element methods for advective-diffusive problems. *Int. J. Num. Meth. Fluids* 1999; **31**:203–221.

Oñate E. A stabilized finite element method for incompressible viscous flows using a finite increment calculus formulation. *Comput. Methods Appl. Mech. Engrg.* 2000; **182 (1–2)**:355–370.

Oñate E and Manzan M. Stabilization techniques for finite element analysis of convection diffusion problems. In *Computational Analysis of Heat Transfer*, Comini G and Sunden B (eds), WIT Press: Southampton, 2000.

Oñate E and García J. A finite element method for fluid-structure interaction with surface waves using a finite calculus formulation. *Comput. Methods Appl. Mech. Engrg.* 2001; **191**:635–660.

Oñate E. Possibilities of finite calculus in computational mechanics. Submitted to *Int. J. Num. Meth. Engng*, 2002.

Oñate E. A general stabilized formulation for incompressible fluid flow using finite calculus and the finite element method. In *Towards a New Fluid Dynamics with its Challenges in Aeronautics*, Periaux J, Chamption D, Pironneau O and Thomas Ph. (eds), CIMNE, Barcelona, Spain 2002.

Peraire J, Morgan K and Peiro J. The simulation of 3D incompressible flows using unstructured grids. In *Frontiers of Computational Fluid Dynamics*, Caughey DA and Hafez MM. (eds), Chapter 16, J. Wiley, 1994.

Pironneau O. On the transport-diffusion algorithm and its applications to the Navier-Stokes equations. *Numer. Math.* 1982; **38**:309.

Raven H. A solution method for the nonlinear ship resistance problem. *Doctoral Thesis*, Maritime Research Institute, Netherlands, 1996.

Reed AM, Telste JG, Scragg CA and Liepmann D. Analysis of transon stern flows. *Proc. 17th Symp. on Naval Hidrodynamics*, The Hague, The Netherlands, 1990.

Sheng C, Taylor LK and Whitfield DL. Implicit lower-upper/approximate-factorization schemes for incompressible flows. *Journal of Computational Physics* 1996; **128 (1)**:32–42.

Soding H. Advances in panel methods. *Proc. of the 21th Symp. on Naval Hidrodynamics*, Trondheim, Norway, 1996.

Encyclopedia of Computational Mechanics. Edited by Erwin Stein, René de Borst and Thomas J.R. Hughes.

Storti M, Nigro N and Idelsohn SR. Steady state incompressible flows using explicit schemes with an optimal local preconditioning. *Comput. Meth. Appl. Mech. and Engrg.* 1995; **124**:231–252.

Storti M, Nigro N, Idelsohn SR. Equal order interpolations. A unified approach to stabilize the incompressible and convective effects. *Comput. Meth. Appl. Mech. and Engrg.* 1997; **143**:317–331.

Tdyn. A finite element code for fluid-dynamic analysis, COMPASS Ingeniería y Sistemas SA, www.compassis.com, (2002).

Tezduyar TE. Stabilized finite element formulations for incompressible flow computations. *Advances in Applied Mechanics* 1991; **28**:1–44.

Tezduyar TE, Mittal S, Ray SE and Shih R. Incompressible flow computations with stabilized bilinear and linear equal order interpolation velocity–pressure elements. *Comput. Methods Appl. Mech. Engrg.* 1992; **95**:221–242.

Tezduyar TE, Behr M and Liou J. A new strategy for finite element computations involving moving boundaries and interfaces - the deforming-spatial-domain/space-time procedure: I. The concept and the preliminary tests. *Comput. Methods in Appl. Mech. and Engrg.* 1992; **94**:339–351.

Tezduyar TE. Finite element methods for flow problems with moving boundaries and interfaces. *Arch. Comput. Meth. Engng.* 2001; **8**:83–130.

Wehausen JV. The wave resistance of ships. *Advances in Applied Mechanics*, 1973.

Wigley. Comparative experiment on Wigley parabolic models in Japan. 17th ITTC Resistance Committee Report, 2nd ed., 1983.

Wilcox DC. *Turbulence modeling for CFD.* DCW Industries Inc., 1994.

Xia F. Numerical calculation of ship flows with special emphasis on the free surface potential flow. *Doctoral Thesis*, Chalmers University of Technology, Sweden, 1986.

Zienkiewicz OC and Taylor RC. *The finite element method*, 5th Edition, 3 Volumes, Butterworth–Heinemann, 2000.

Zienkiewicz OC and Codina R. A general algorithm for compressible and incompressible flow. Part I: The split characteristic based scheme. *Int. J. Num. Meth. in Fluids* 1995; **20**:869–85.

Encyclopedia of Computational Mechanics. Edited by Erwin Stein, René de Borst and Thomas J.R. Hughes.

LIST OF FIGURES

Encyclopedia of Computational Mechanics. Edited by Erwin Stein, René de Borst and Thomas J.R. Hughes.

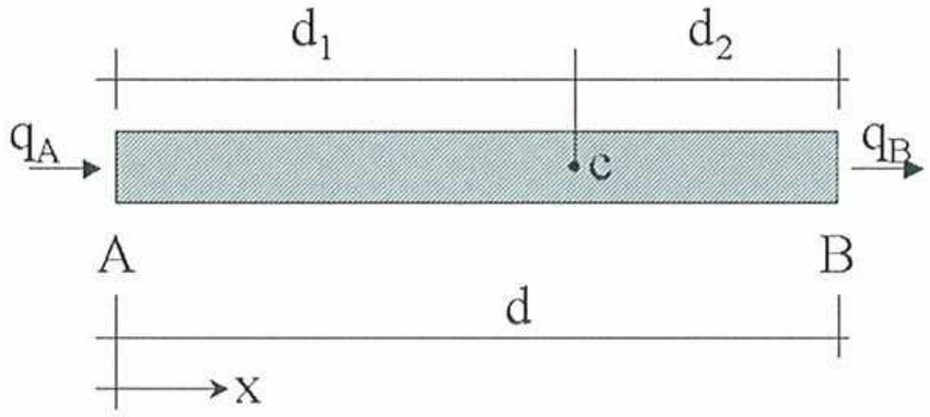

Figure 1. Equilibrium of fluxes in a balance domain of finite size

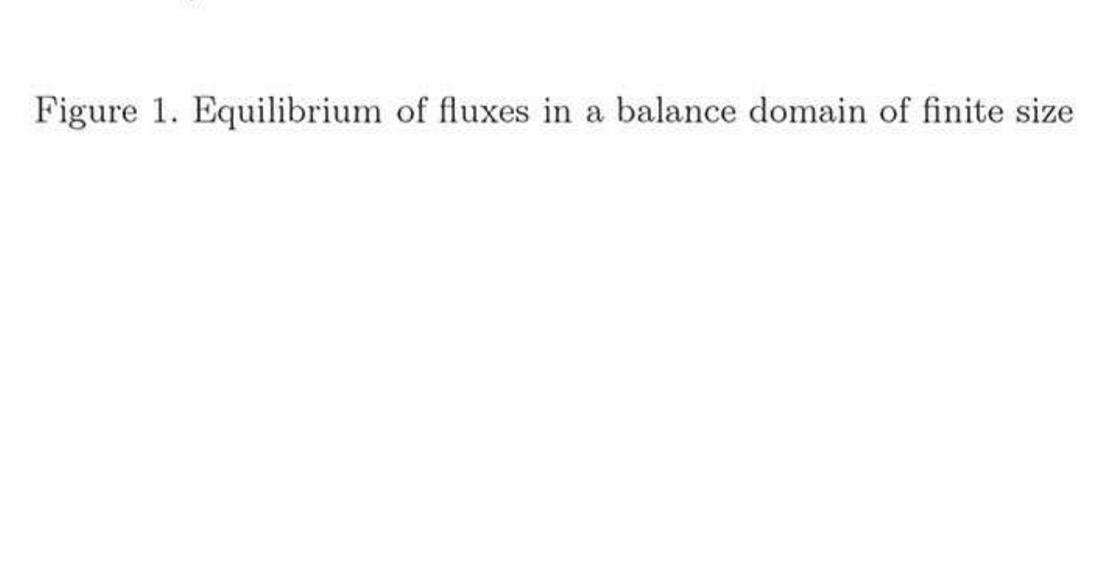

Figure 2. Reference surface for the wave height β

Encyclopedia of Computational Mechanics. Edited by Erwin Stein, René de Borst and Thomas J.R. Hughes.

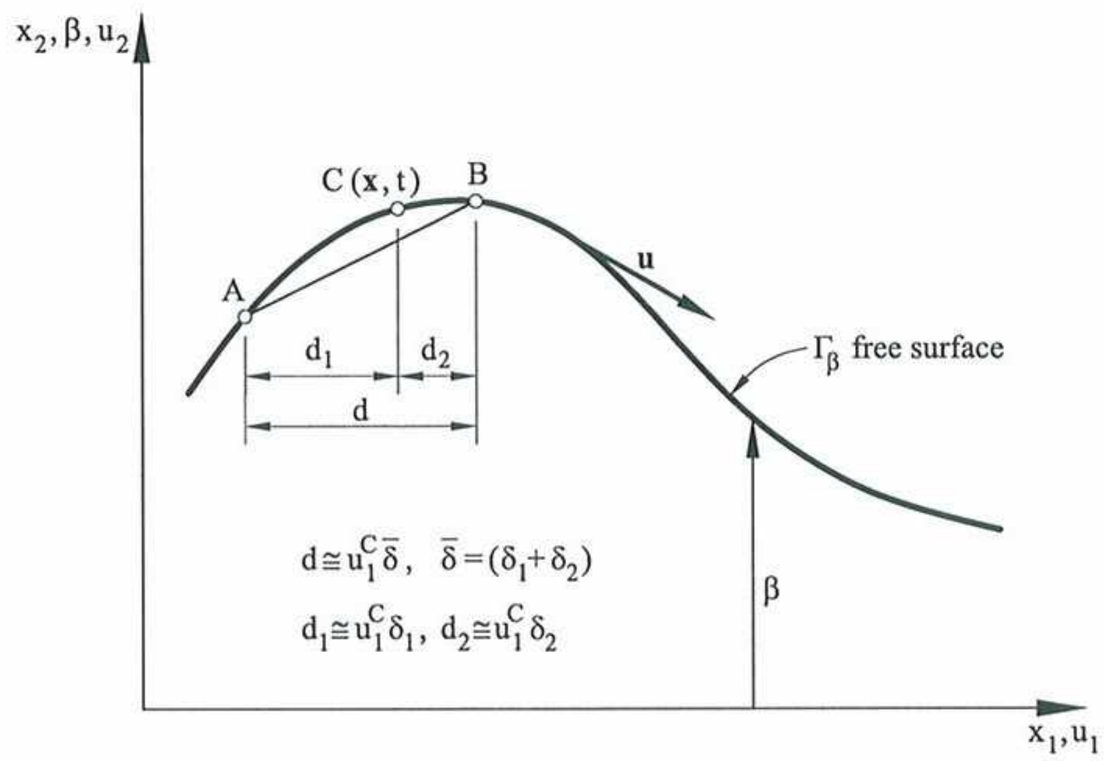

Figure 3. Definition of free surface parameters

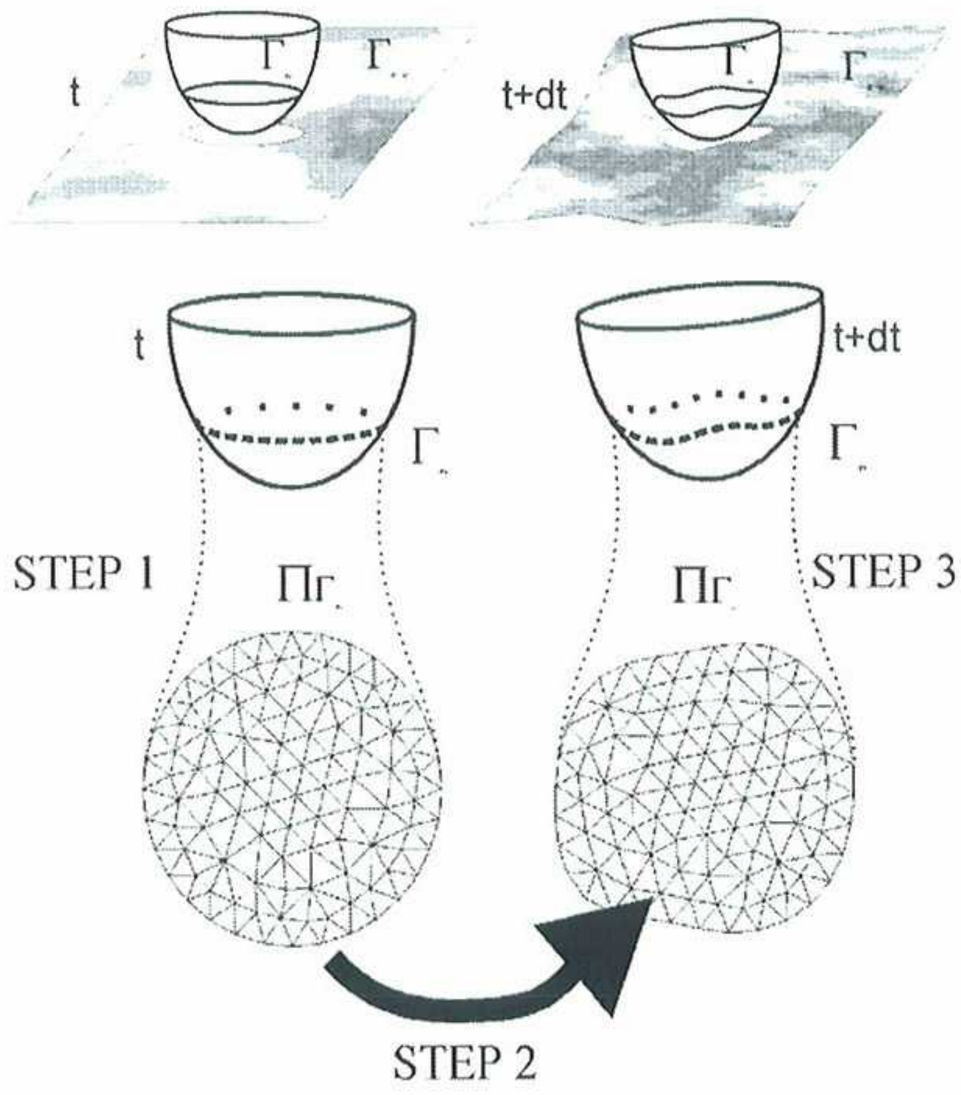

Figure 4. Changes on the fluid interface in a floating body

Encyclopedia of Computational Mechanics. Edited by Erwin Stein, René de Borst and Thomas J.R. Hughes.

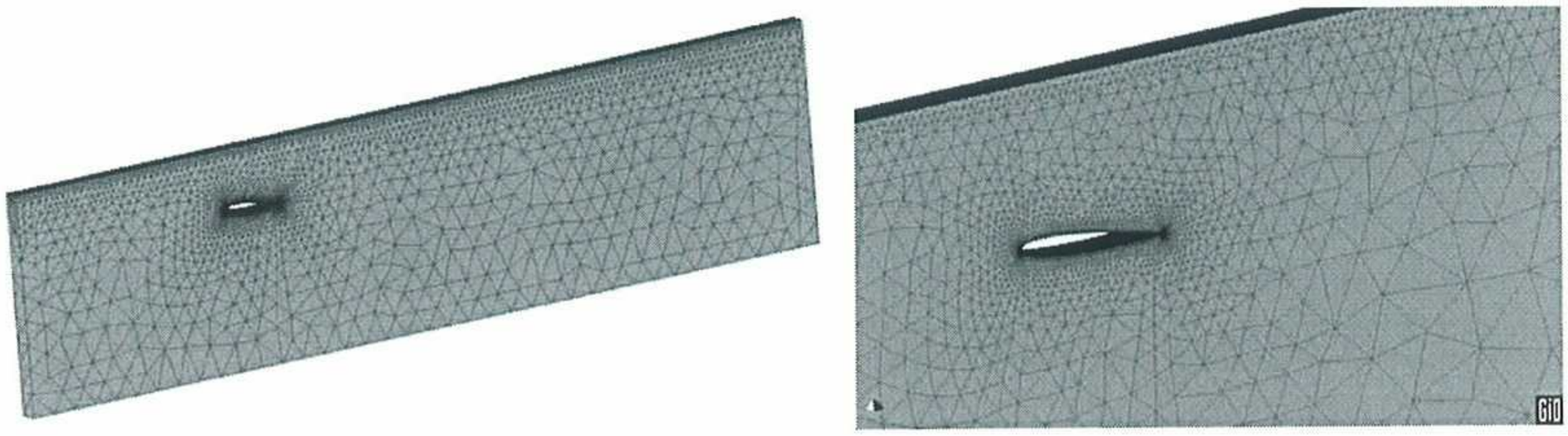

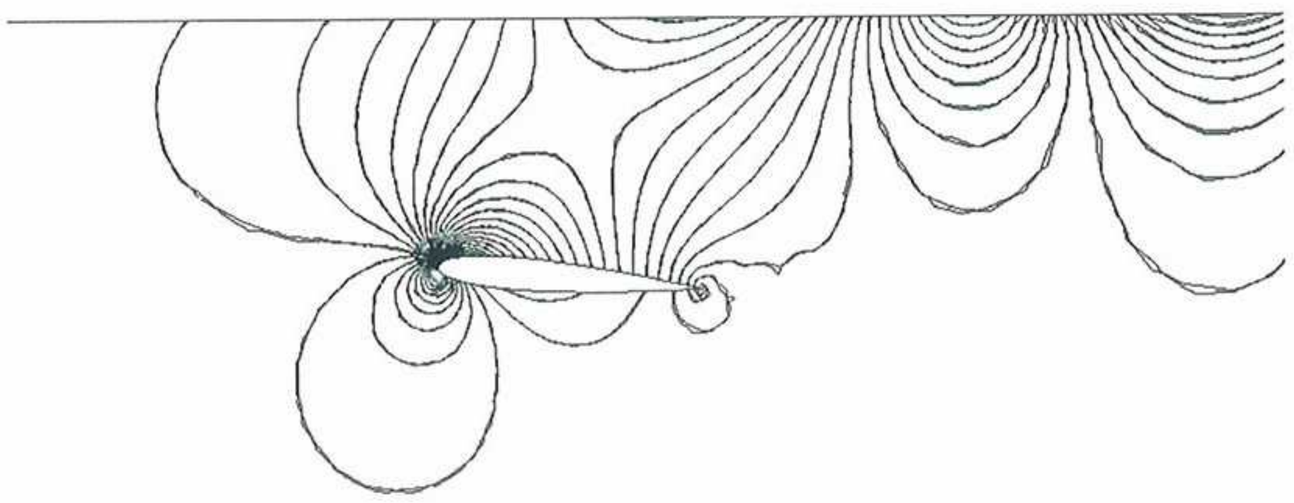

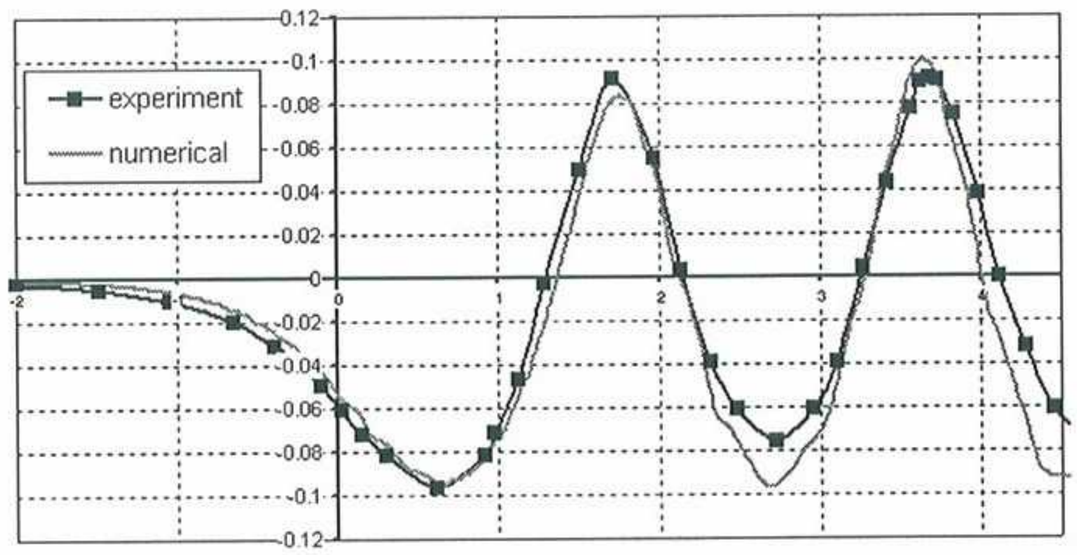

Figure 5. Submerged NACA0012 profile. a) Detail of the mesh of 70000 linear tetrahedra chosen. b) Pressure contours. c) Stationary wave profile

Encyclopedia of Computational Mechanics. Edited by Erwin Stein, René de Borst and Thomas J.R. Hughes.

a)

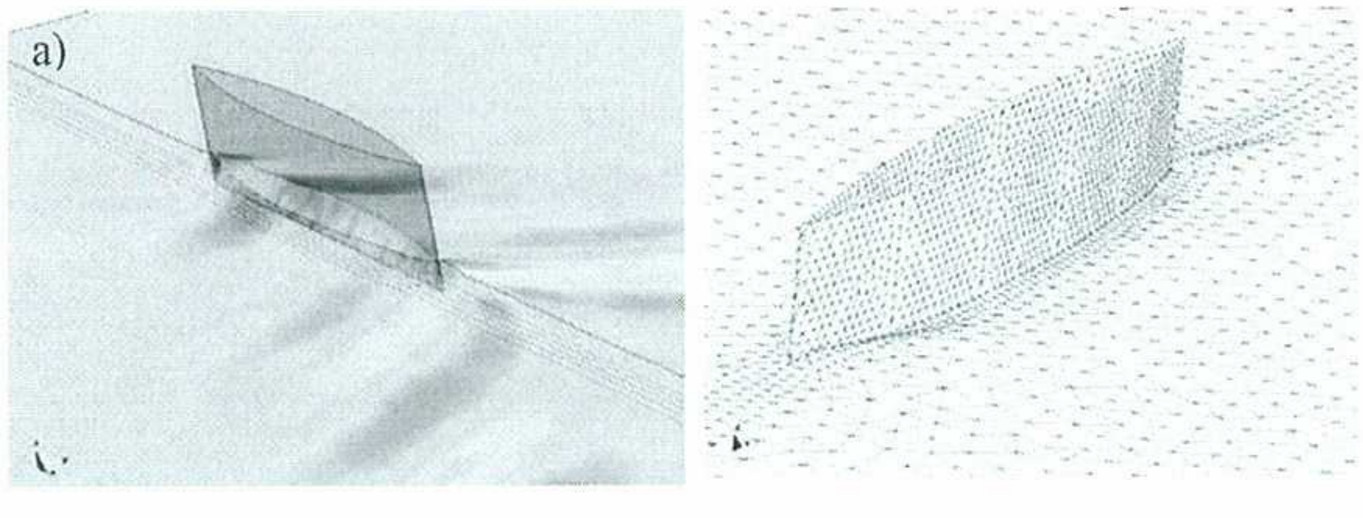

b)

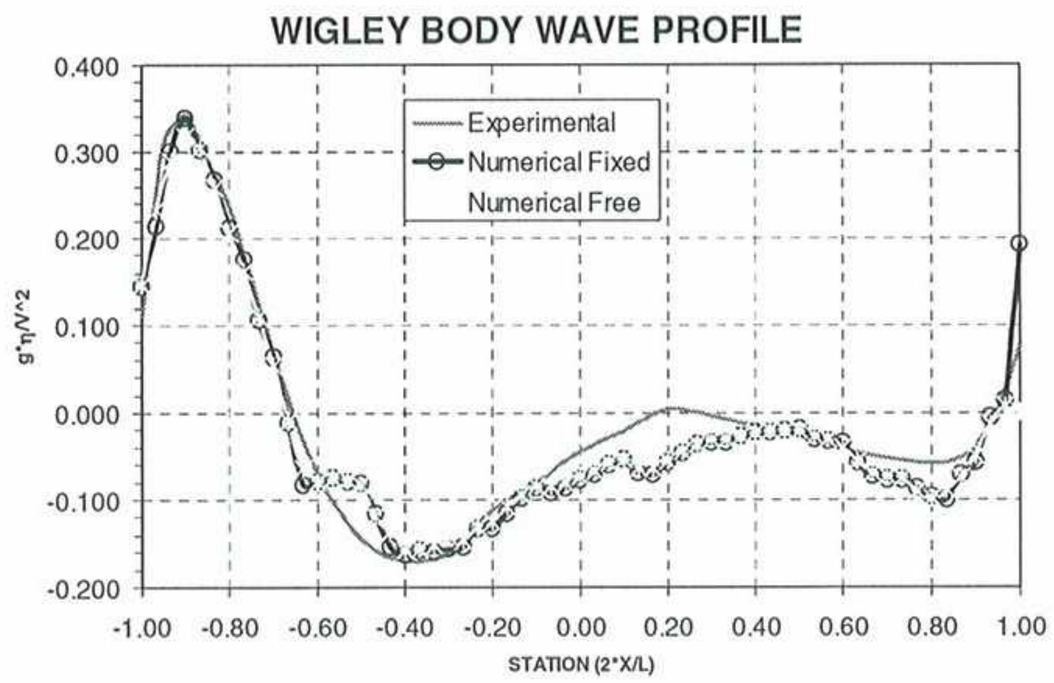

c)

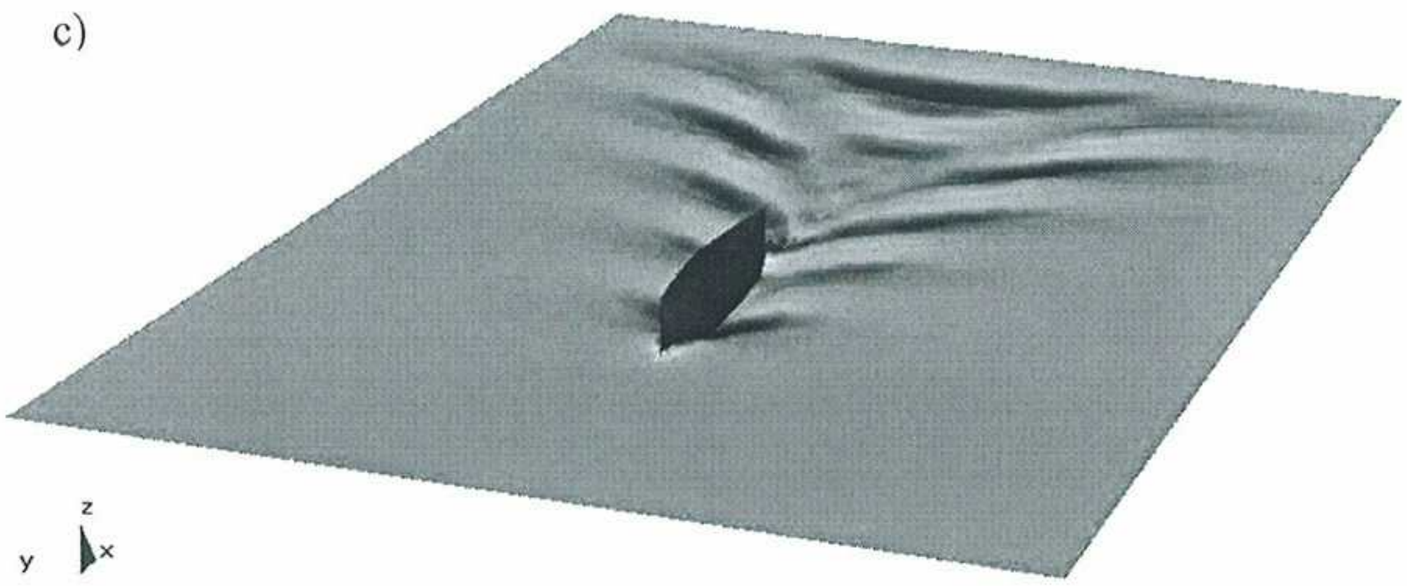

Figure 6. Wigley hull. a) Pressure distribution and mesh deformation of the wigley hull (free model). b) Numerical and experimental body wave profiles. c) Free surface contours for the truly free ship motion

Encyclopedia of Computational Mechanics. Edited by Erwin Stein, René de Borst and Thomas J.R. Hughes.

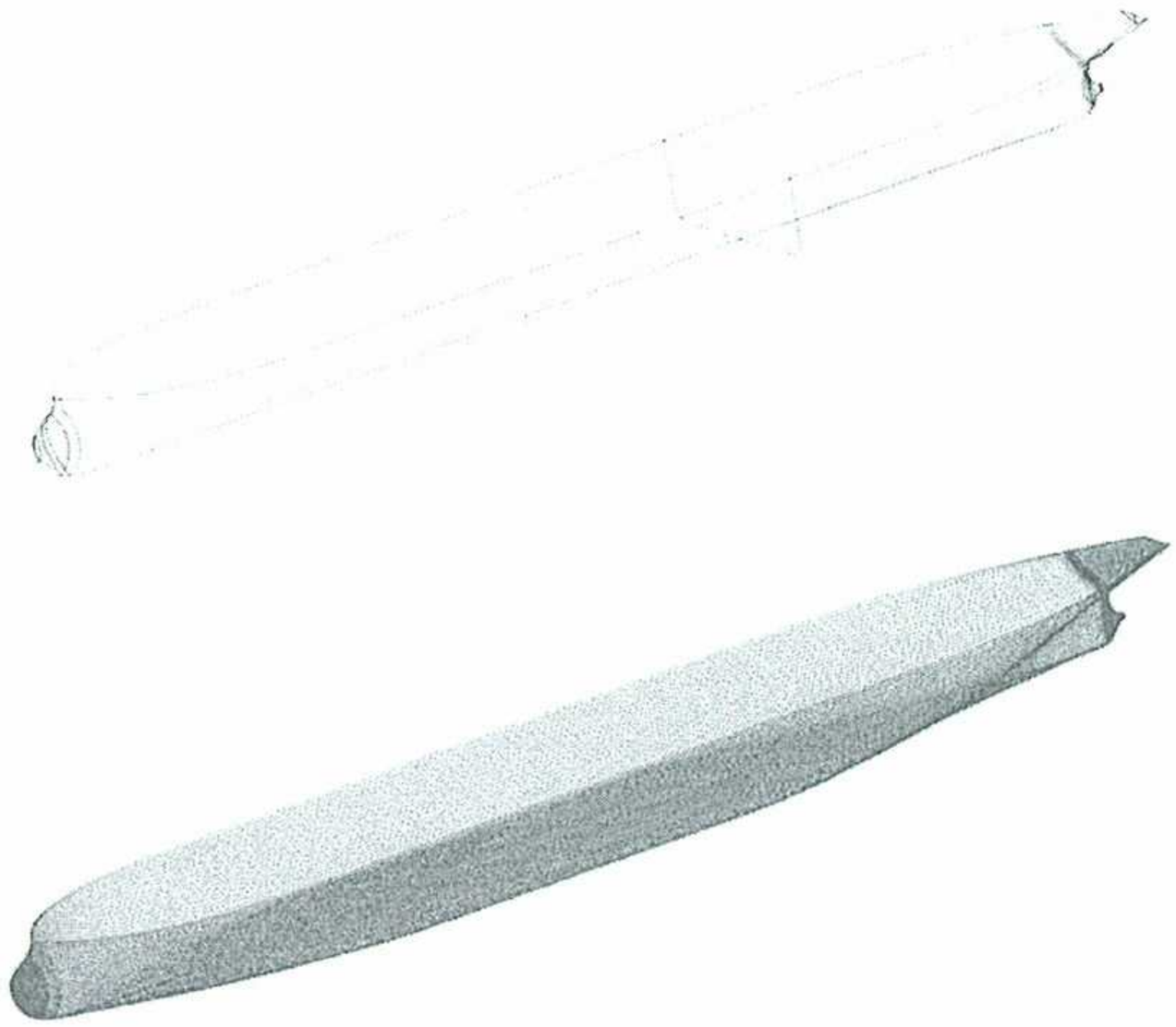

Figure 7. KVLCC2 model. Geometrical definition based on NURBS surfaces and surface mesh used in the analysis

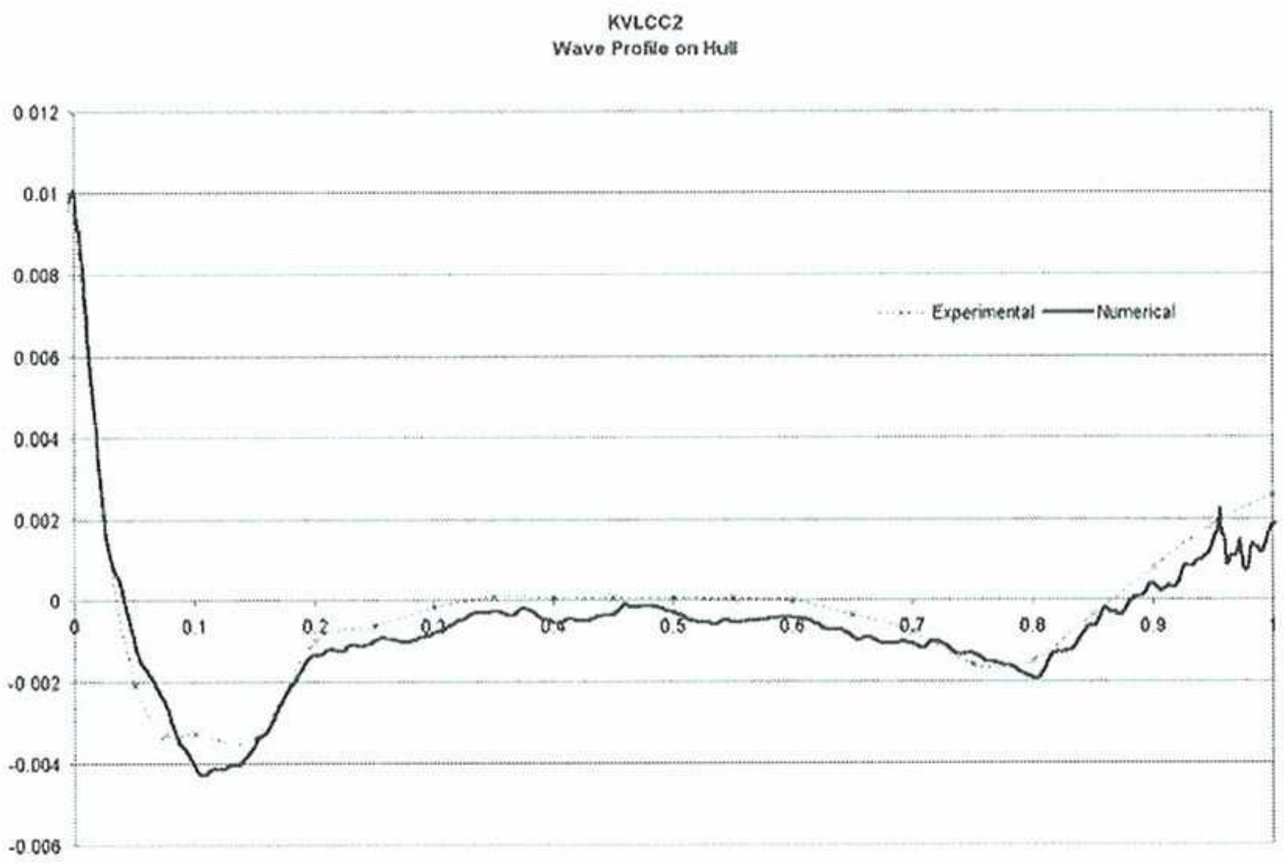

Figure 8. KVLCC2 model. Wave profile on the hull. Thick line shows numerical results

Encyclopedia of Computational Mechanics. Edited by Erwin Stein, René de Borst and Thomas J.R. Hughes.

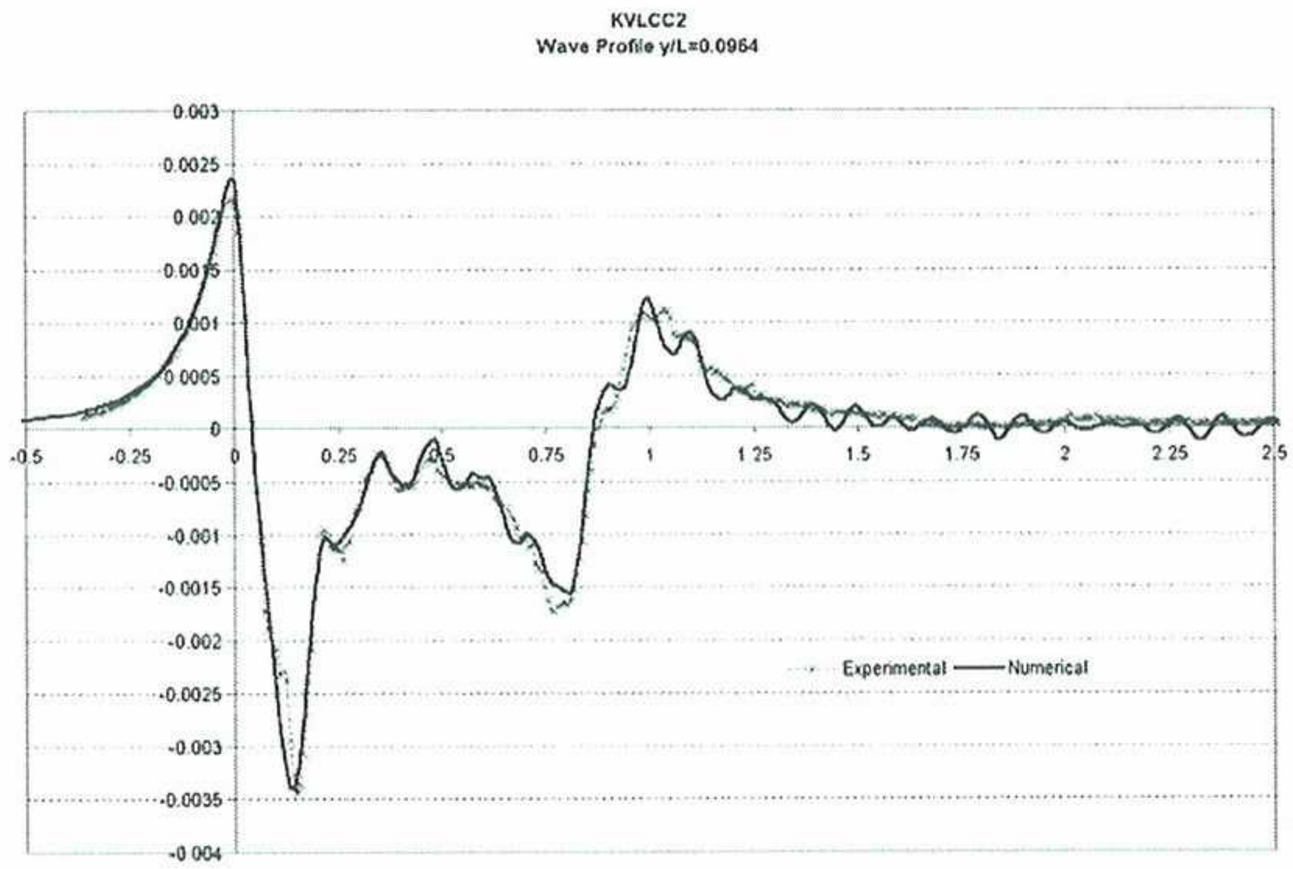

Figure 9. KVLCC2 model. Wave profile on a cut at y/L=0.0964. Thick line shows numerical results

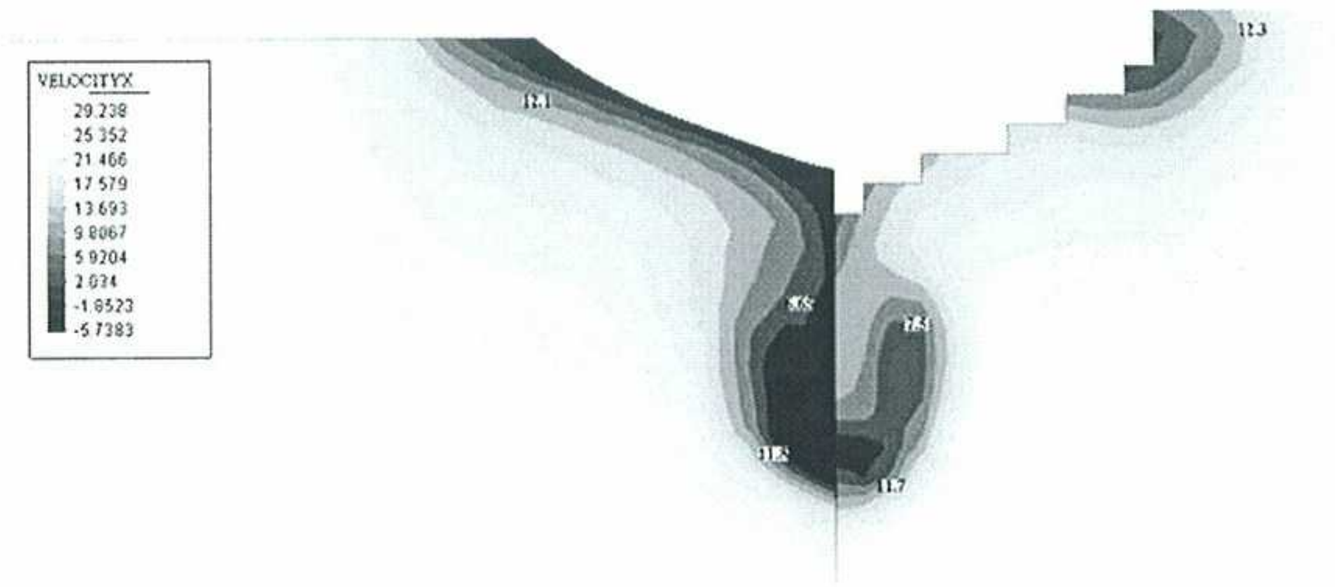

Figure 10. KVLCC2 model. Map of the X component of the velocity on a plane at 2.71 m from the orthogonal aft. Experimental data shown in the right

Encyclopedia of Computational Mechanics. Edited by Erwin Stein, René de Borst and Thomas J.R. Hughes.

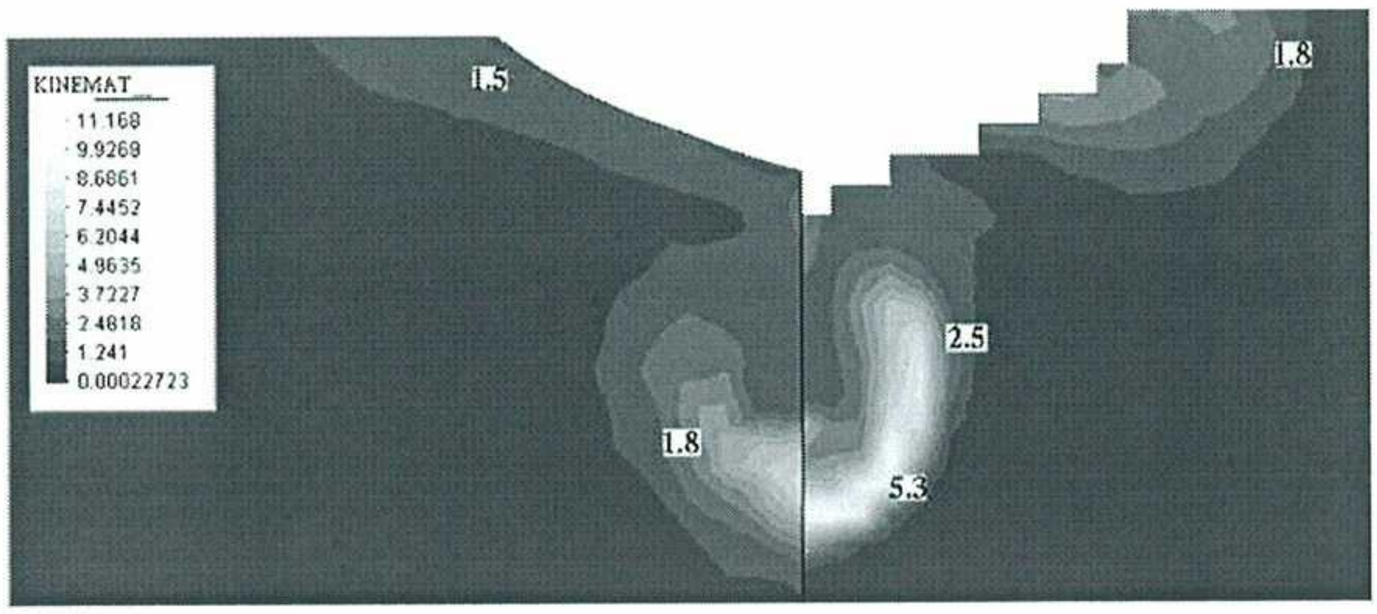

Figure 11. KVLCC2 model. Map of the eddy kinetic energy (K) on a plane at 2.71 m from the orthogonal aft. Experimental data shown in the right

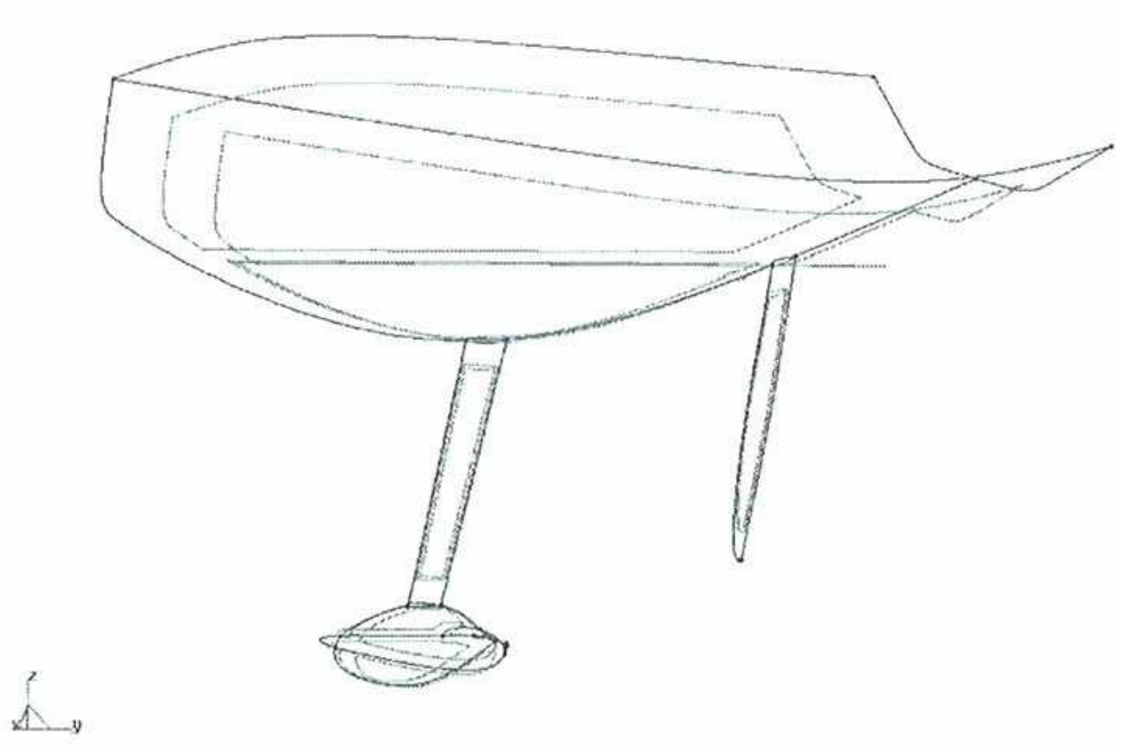

Figure 12. NURBS-based geometry used in the analysis of the Rioja de España America Cup boat

Encyclopedia of Computational Mechanics. Edited by Erwin Stein, René de Borst and Thomas J.R. Hughes.

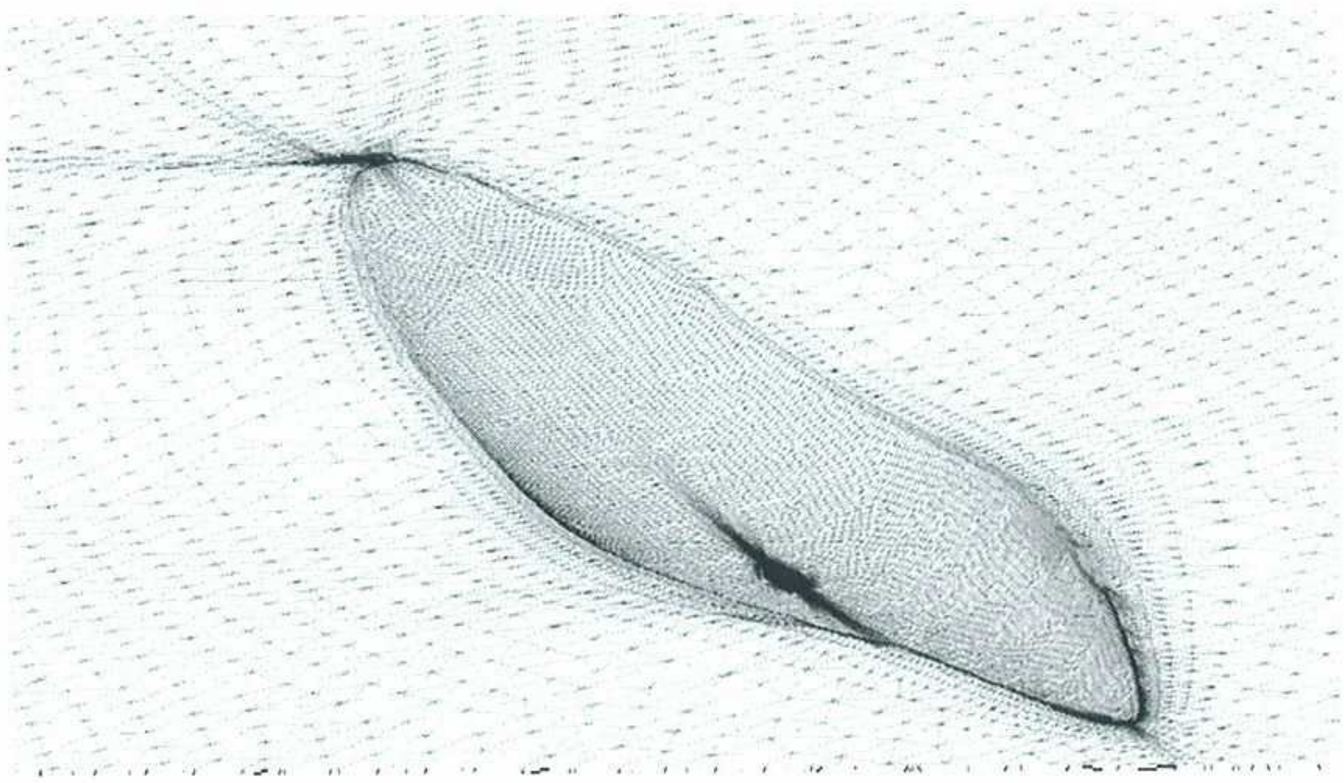

Figure 13. Detail of the final (boundary) mesh used in the E0D0 case. The mesh has been adapted taking into account sinkage, trim and free surface deformation

Figure 14. Detail of the mesh used in the analysis of the E0D0 case, around keel-bulb union

Encyclopedia of Computational Mechanics. Edited by Erwin Stein, René de Borst and Thomas J.R. Hughes.

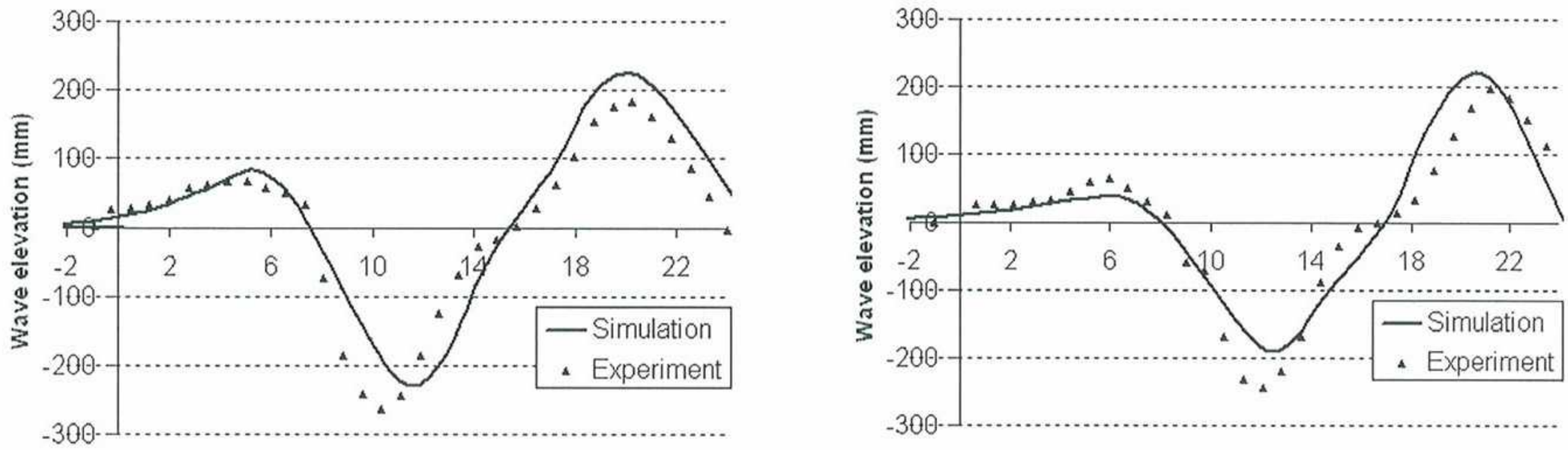

Figure 15. Wave elevation profile for 10kn (left: E0D0, right: E15D2)

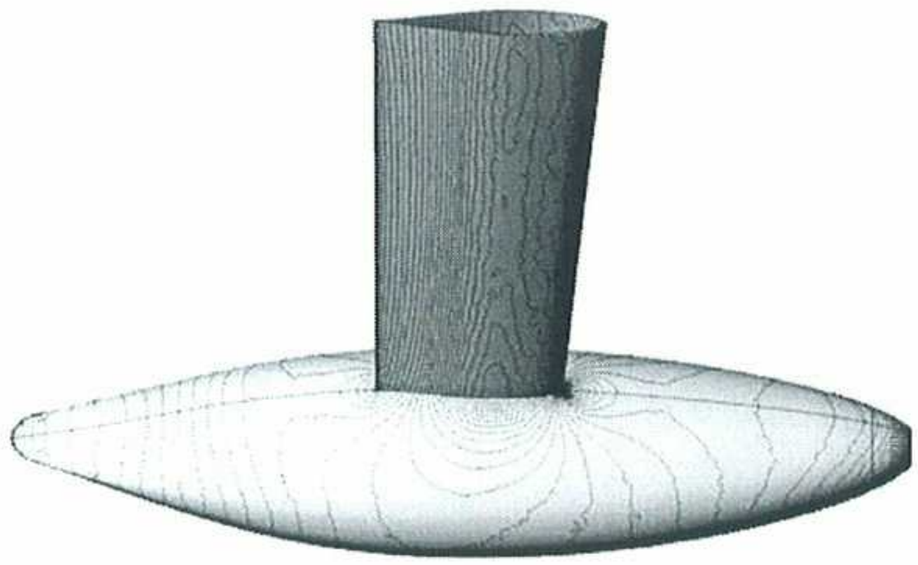

Figure 16. E0D0 8kn. Pressure contours on bulb

Encyclopedia of Computational Mechanics. Edited by Erwin Stein, René de Borst and Thomas J.R. Hughes.

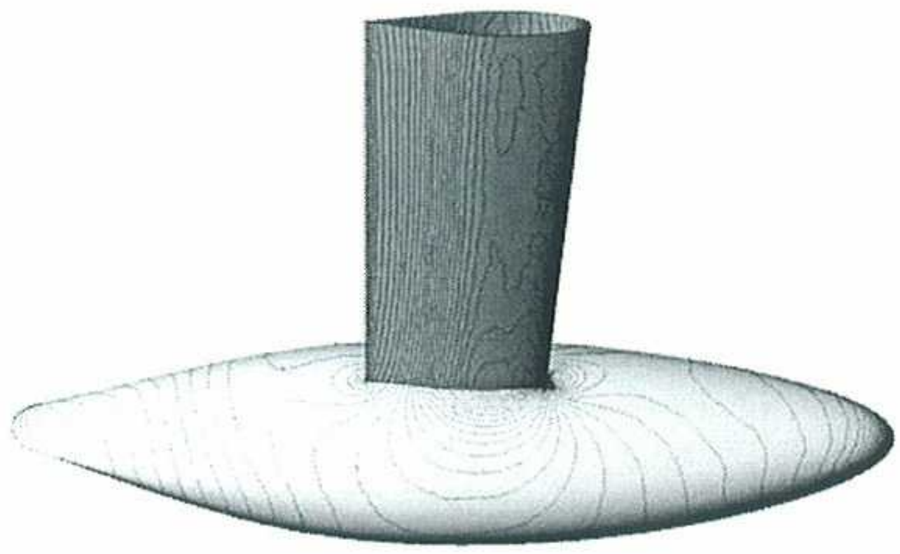

Figure 17. E25D2 8kn. Pressure contours on bulb

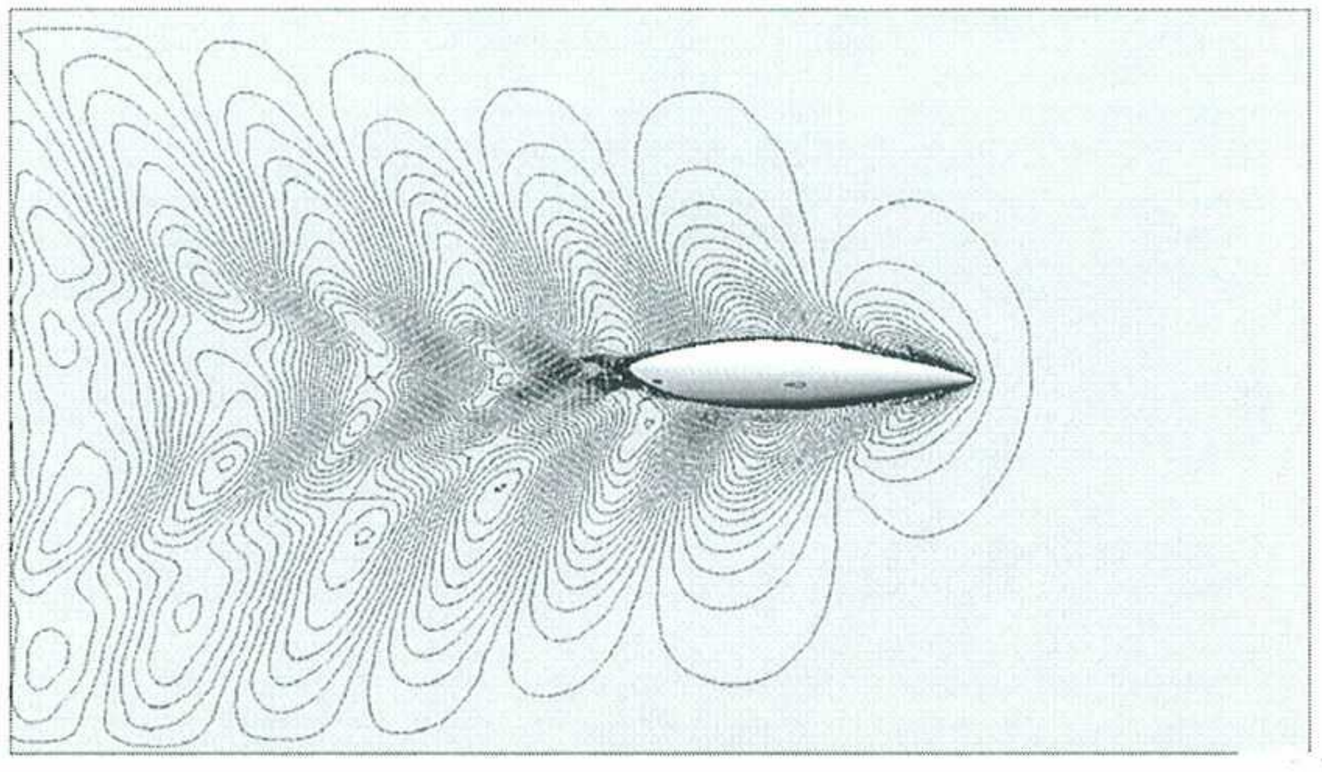

Figure 18. E15D2 9kn Wave map

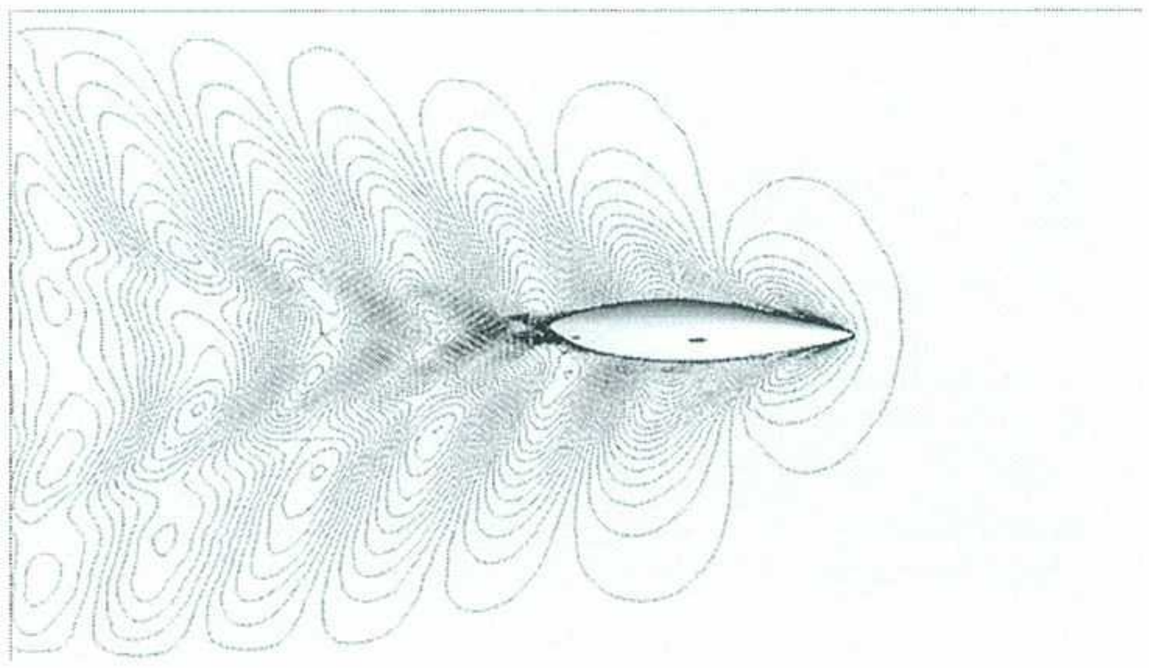

Figure 19. E25D2 9kn Wave map

Figure 20. E15D2 7.5 kn. Pressure map on appendages and streamlines. Perspective view

Encyclopedia of Computational Mechanics. Edited by Erwin Stein, René de Borst and Thomas J.R. Hughes.

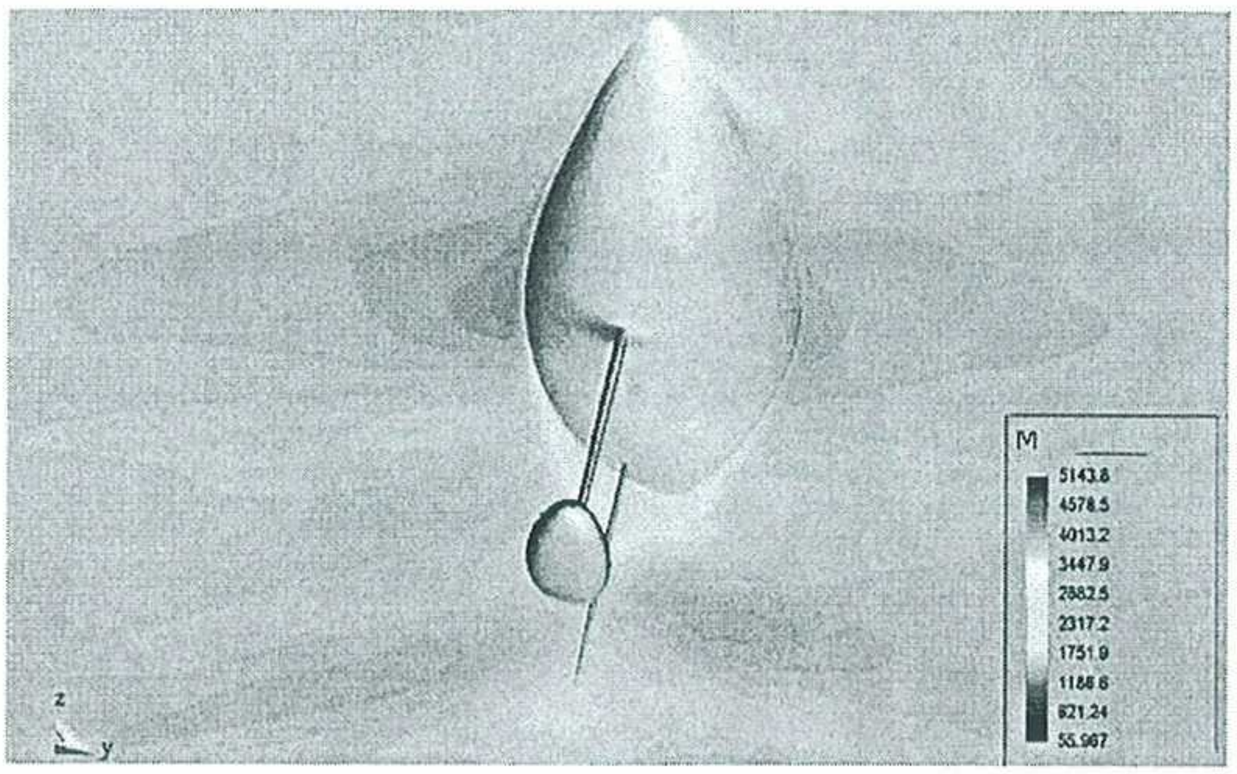

Figure 21. E15D4 7.5 kn. Velocity modulus contours. Perspective view

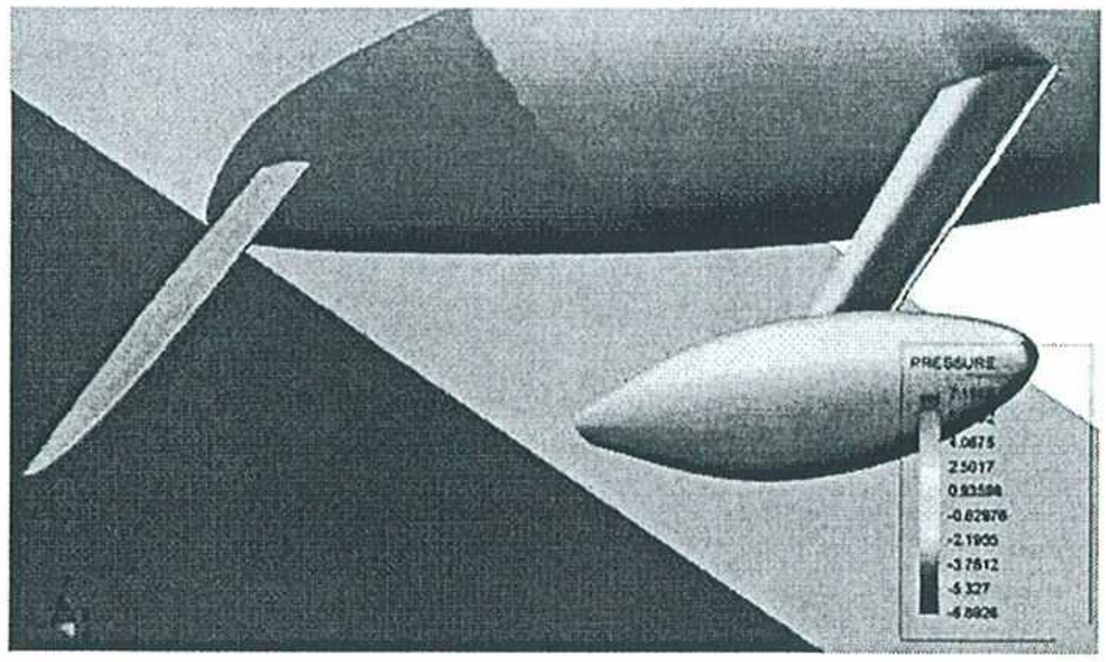

Figure 22. E25D2 7.5 kn. Pressure contours on appendages and cuts. Perspective view

Encyclopedia of Computational Mechanics. Edited by Erwin Stein, René de Borst and Thomas J.R. Hughes.

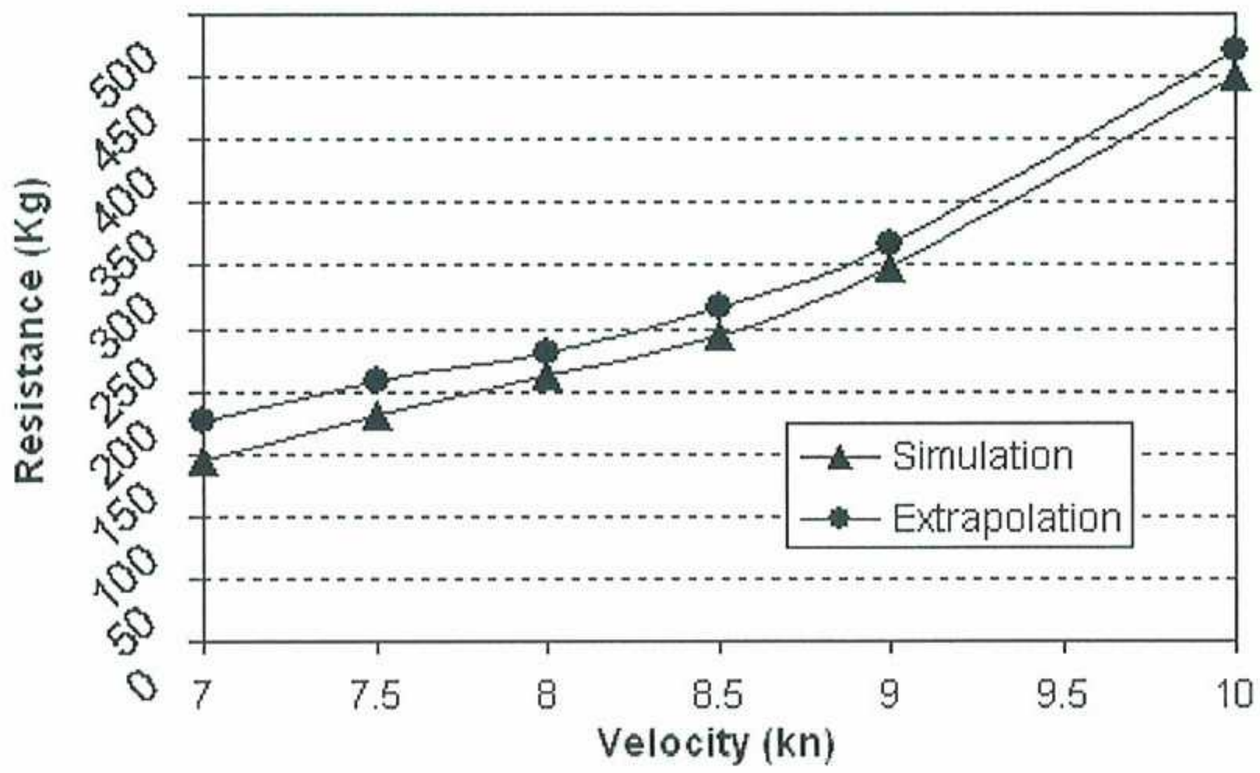

Figure 23. E0D0. Resistance graph. Comparison with results extrapolated from experimental data

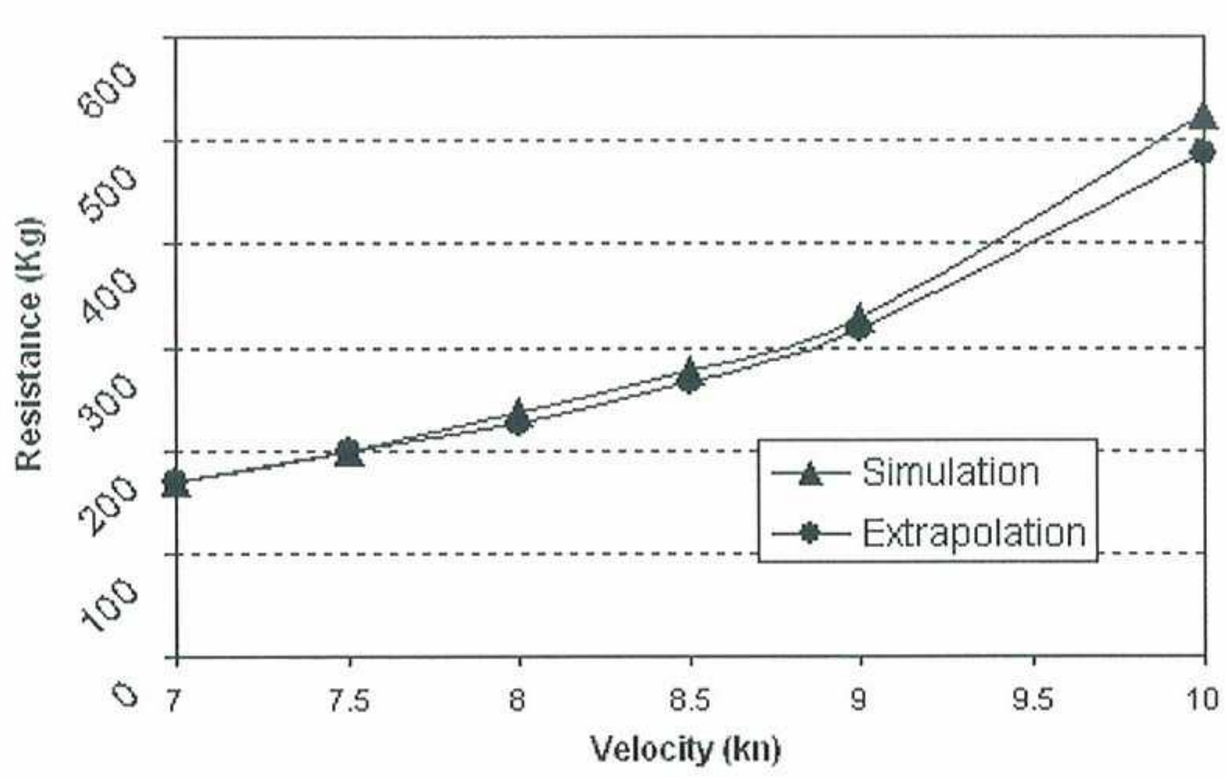

Figure 24. E15D4. Resistance graph. Comparison with results extrapolated from experimental data

Encyclopedia of Computational Mechanics. Edited by Erwin Stein, René de Borst and Thomas J.R. Hughes.

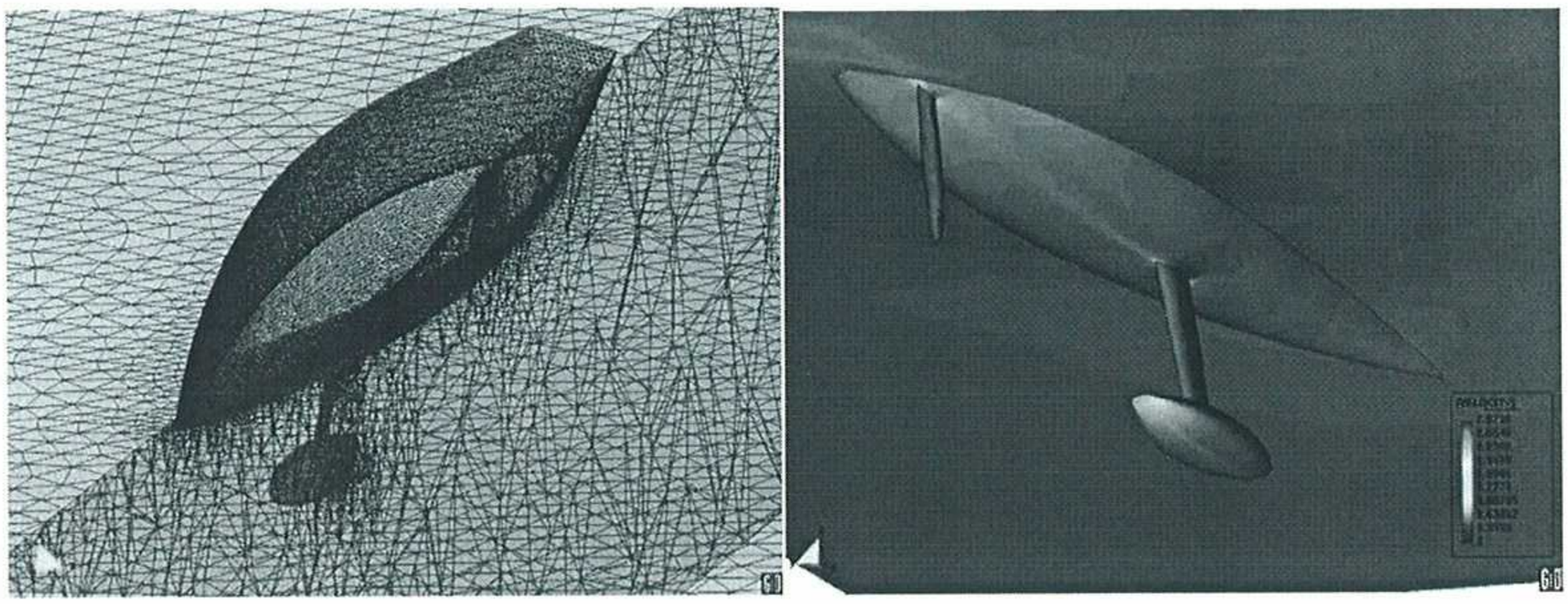

Figure 25. American Cup *Bravo España* racing sail boat. a) Mesh used in the analysis. b) Velocity contours

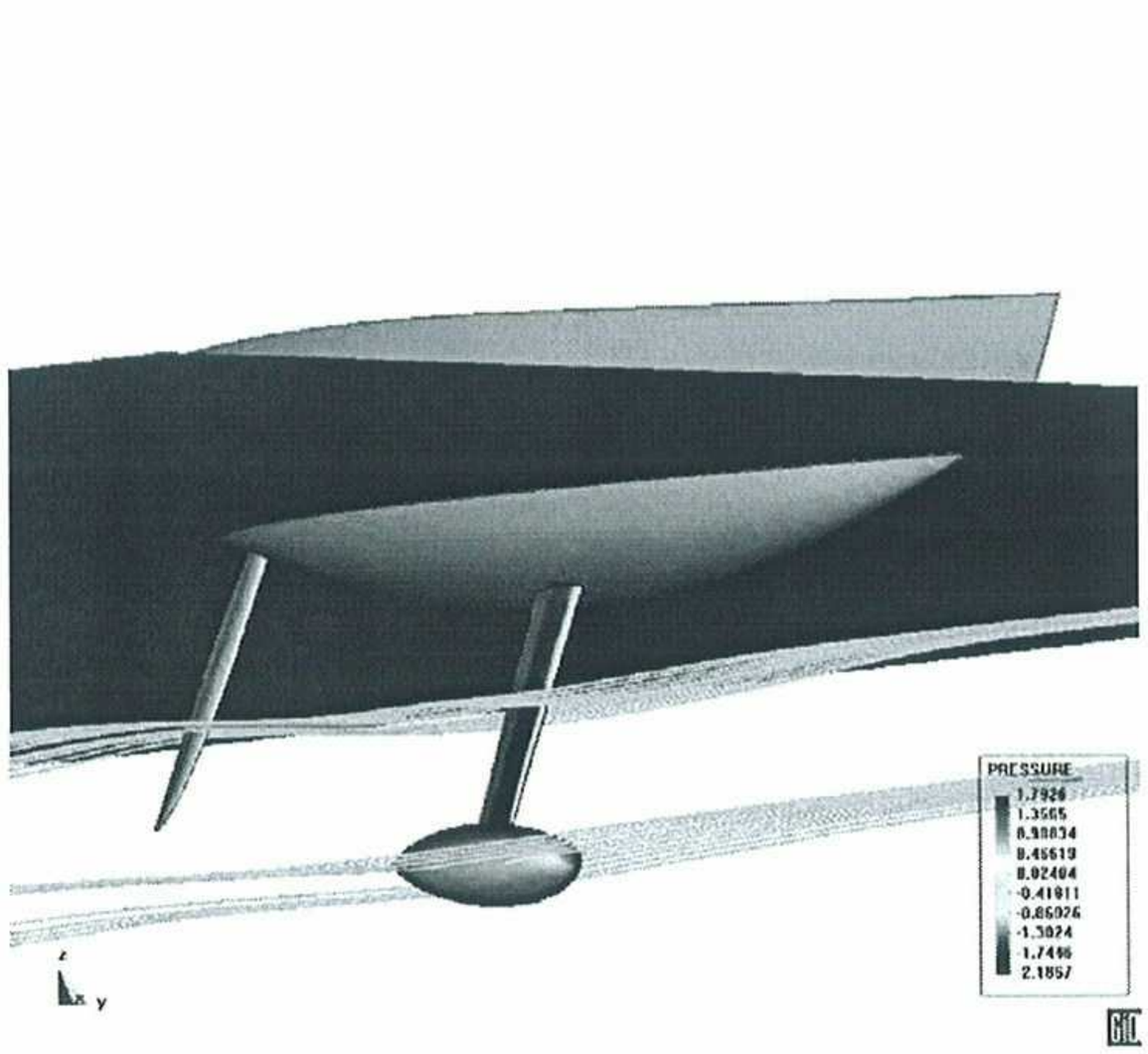

Figure 26. *Bravo España*. Streamlines

Encyclopedia of Computational Mechanics. Edited by Erwin Stein, René de Borst and Thomas J.R. Hughes.

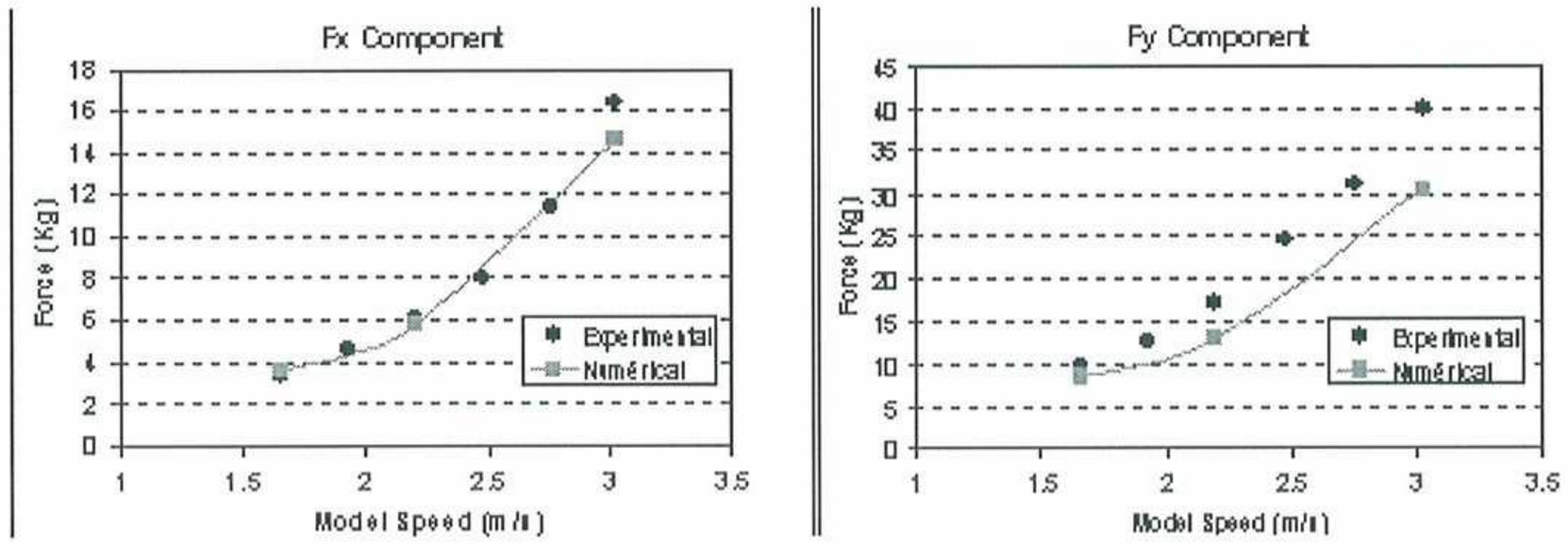

Figure 27. *Bravo España*. Resistance test. Comparison of numerical results with experimental data

Encyclopedia of Computational Mechanics. Edited by Erwin Stein, René de Borst and Thomas J.R. Hughes.

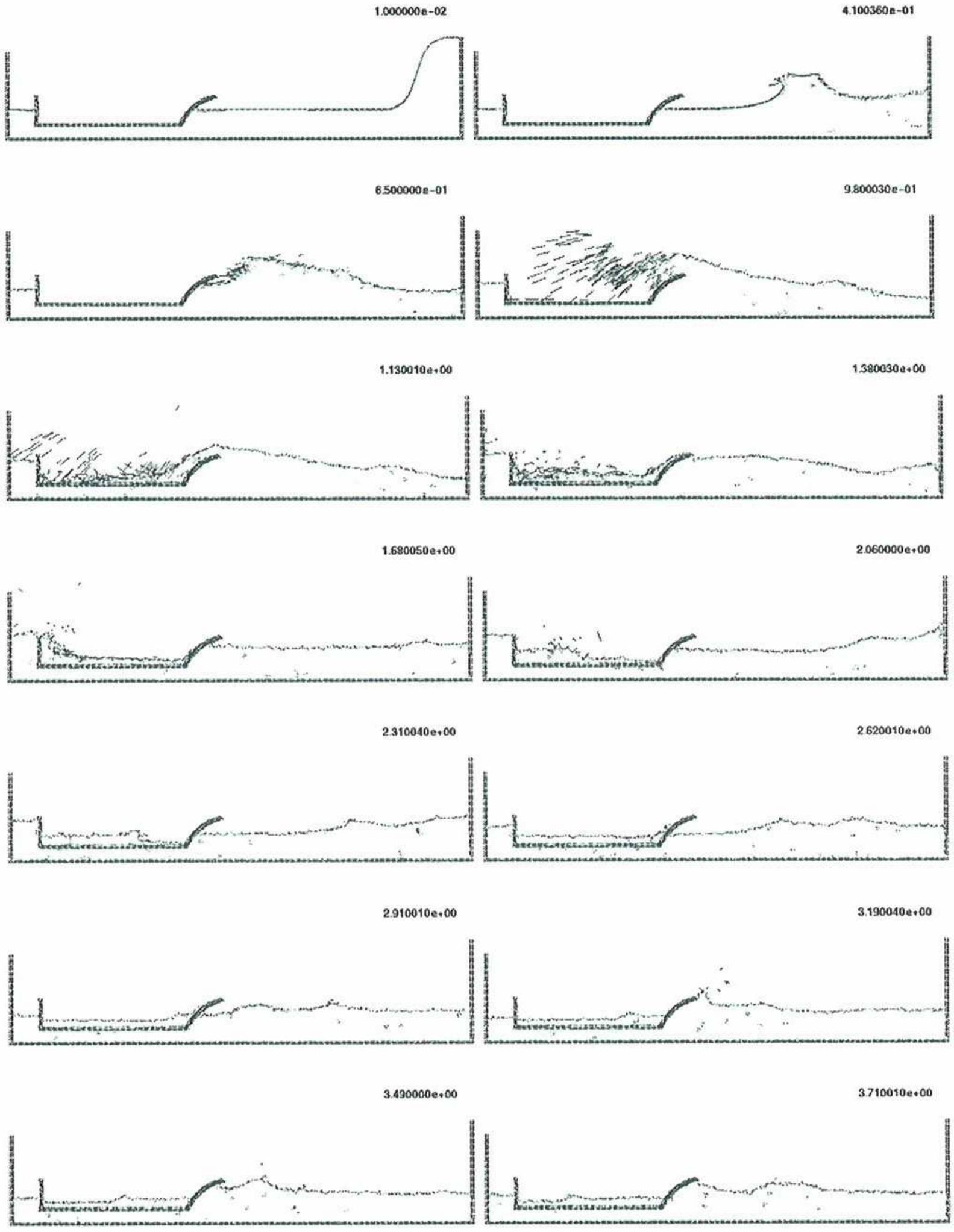

Figure 28. Fixed ship under external waves

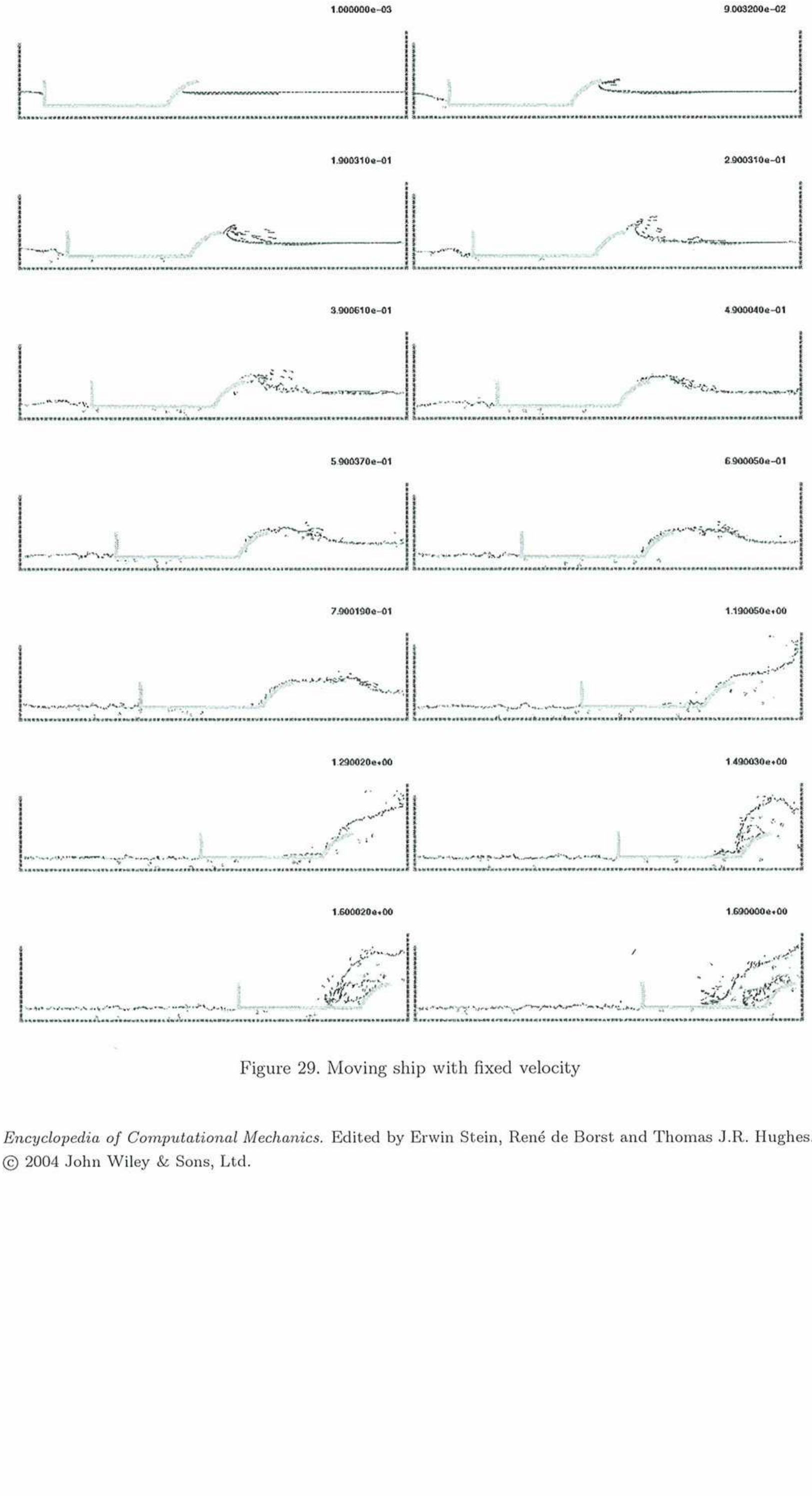

Figure 29. Moving ship with fixed velocity

Encyclopedia of Computational Mechanics. Edited by Erwin Stein, René de Borst and Thomas J.R. Hughes.

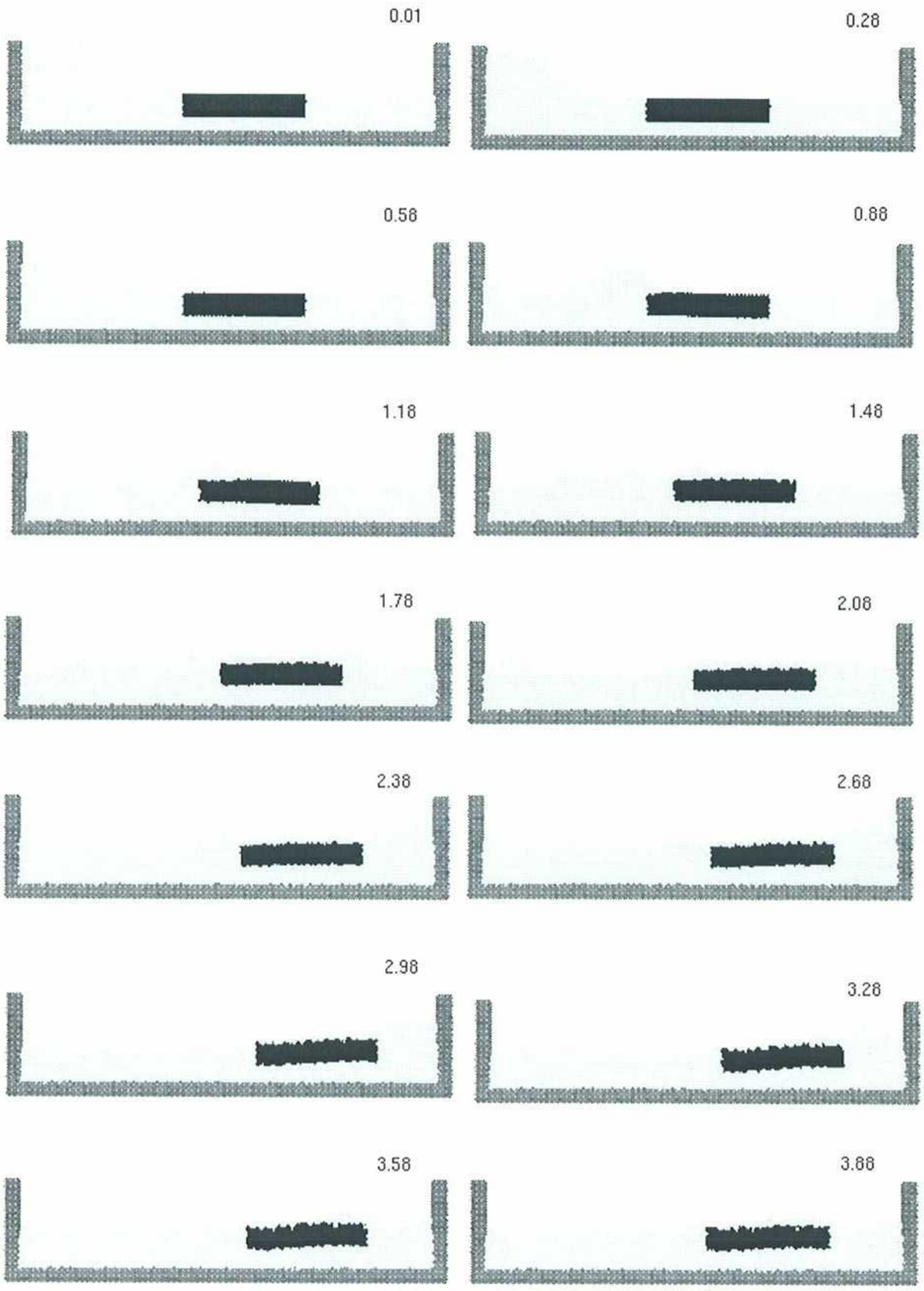

Figure 30. Floating solid hit by a wave

Encyclopedia of Computational Mechanics. Edited by Erwin Stein, René de Borst and Thomas J.R. Hughes.